Available online at www.sciencedirect.com
SCIENCE DIRECT
ELSEVIER
Biochemical and Biophysical Research Communications 342 (2006) 766–772
BBRC
www.elsevier.com/locate/ybbrc

Periostin is an extracellular matrix protein required for eruption of incisors in mice

Isao Kii [a], Norio Amizuka [b], Li Minqi [b], Satoshi Kitajima [c], Yumiko Saga [d], Akira Kudo [a,*]

[a] *Department of Biological Information, Tokyo Institute of Technology, Yokohama 226-8501, Japan*
[b] *Center for Transdisciplinary Research, Niigata University, Niigata 951-8514, Japan*
[c] *Division of Cellular and Molecular Toxicology, National Institute of Health Science, Tokyo 158-8501, Japan*
[d] *Division of Mammalian Development, National Institute of Genetics, Mishima 411-8540, Japan*

Received 27 January 2006
Available online 14 February 2006

Abstract

A characteristic tooth of rodents, the incisor continuously grows throughout life by the constant formation of dentin and enamel. Continuous eruption of the incisor is accompanied with formation of shear zone, in which the periodontal ligament is remodeled. Although the shear zone plays a role in the remodeling, its molecular biological aspect is barely understood. Here, we show that periostin is essential for formation of the shear zone. *Periostin*$^{-/-}$ mice showed an eruption disturbance of incisors. Histological observation revealed that deletion of *periostin* led to disappearance of the shear zone. Electron microscopy revealed that the disappearance of the shear zone resulted from a failure in digestion of collagen fibers in the *periostin*$^{-/-}$ mice. Furthermore, immunohistochemical analysis using anti-periostin antibodies demonstrated the restricted localization of periostin protein in the shear zone. Periostin is an extracellular matrix protein, and immunoelectron microscopy showed a close association of periostin with collagen fibrils in vivo. These results suggest that periostin functions in the remodeling of collagen matrix in the shear zone.

Keywords: Periostin; Incisor; Collagen; Eruption; Periodontal ligament; Shear zone; Tooth; Fasciclin

The periodontal ligament is a dense connective tissue containing fibroblastic cells and vascular and neural elements [1,2]. Thick collagen bundles, i.e., principal periodontal fibers, run between the cementum and alveolar bone, and some of them penetrate into these tissues as Sharpey's fibers. The periodontal ligament serves as a cushion as well as an anchor between the teeth and the alveolar bone during mastication. Tooth eruption and orthodontic tooth movement induce the active remodeling of the periodontal ligament, following to realignment of teeth. Several MMPs are reported to be involved in the remodeling of the periodontal ligament [3–7].

Rodent's incisors, having a sharp chisel-like shape, differ from other teeth, molars, in certain biological properties: incisors erupt continuously throughout life. The labial portion of these teeth is covered with enamel, and the remaining surface with cementum. Previously, it was reported that the periodontal ligament of the rodent incisor comprises two compartments: a highly vascularized part and an unvascularized part, and these are also called the alveolus-related part and the tooth-related part, respectively [8]. The former, which localizes closer to the alveolar bone, is regarded as the non-moving zone, whereas the latter is the zone that moves during continuous incisor eruption. The boundary between these alveolus- and tooth-related parts is referred to as the shear zone [8]. Synthesis and turnover of total proteins occur throughout the periodontal ligament, whereas remodeling of collagens predominantly occurs in the shear zone [9]. Although the shear zone plays an important role in the remodeling of the periodontal ligament, its molecular biological aspect is barely understood.

* Corresponding author. Fax: +81 45 924 5718.
E-mail address: akudo@bio.titech.ac.jp (A. Kudo).

0006-291X/$ - see front matter © 2006 Elsevier Inc. All rights reserved.
doi:10.1016/j.bbrc.2006.02.016

In the previous studies, we succeeded in identifying an extracellular matrix protein that we termed periostin because of its specific expression patterns in the periosteum and periodontal ligament in adult mice [10–12]. In addition, observations on the fetal mouse demonstrated the expression of periostin in the fascias of muscles, perichondrium, articular surfaces of the epiphyseal cartilage, and joint ligaments [13,14]. Thus, periostin expression is temporally regulated and spatially restricted mostly to the cells of connective tissues, suggesting its potential role in the formation and maintenance of the tendinous connective tissue structures.

In this study, we found that *periostin*$^{-/-}$ mice showed an eruption disturbance of incisors and intended to obtain a mechanistic insight into how the shear zone was maintained in the continuous eruption of incisors.

Materials and methods

Animals. The *periostin*$^{-/-}$ mouse was generated in our laboratory (Kii et al. [15] and Shimazaki et al., manuscript in preparation). Simply, we performed targeted disruption of the periostin gene in mouse embryonic stem (ES) cells using homologous recombination, and the inserted Neo gene was finally deleted in deficient mice by crossing with CAG-Cre mice to excise the neo cassette, and no periostin expression was observed. The *periostin*$^{-/-}$ mice were viable, and the newborns appeared normal. All animals were allowed free access to standard mouse chow and water during the whole experimental period.

Histological analysis. We used four 6-week-old male mice and six 12-week-old male mice homozygous for the disrupted *periostin* gene, and the same number of their wild-type littermates. The mice were perfused through the left ventricle with 4% paraformaldehyde in 0.1 M phosphate buffer (pH 7.4). The mandibles were removed and immersed in the same fixative for an additional 12 h and then decalcified with EDTA solution for 3 weeks. Paraffin sections were prepared and incubated with an antiserum against mouse periostin. Final visualization of immuno-reaction sites was accomplished with 3-3′ diaminobenzidine. Rabbit anti-periostin antibodies were previously described [12].

Immunoelectron microscopy. Cryostat sections obtained from fixed and decalcified specimens were incubated with rabbit polyclonal antisera against mouse periostin and subsequently with HRP-conjugated secondary antibody. The immuno-reactions were visualized with 3-3′ diaminobenzidine. For immunoelectron microscopy, the specimens were processed as described previously [16].

Eruption experiment. To determine if *periostin* would be physiologically involved in the eruption of the incisors, we cut off one of the two lower incisors in the wild-type and the *periostin*$^{-/-}$ mice at the gingival margin. The erupted incisors were then observed 4 days post-operation.

Results

Eruption disturbance of incisors in the periostin$^{-/-}$ *mice*

The *periostin*$^{-/-}$ mice were viable, and the newborns appeared normal. However, as early as 6 weeks after birth, the incisors from the *periostin*$^{-/-}$ mice were shorter than those from the wild-type littermates (data not shown). In 12-week-old wild-type mice, their incisors were nearly adjoined, with only a narrow space between them (Fig. 1A). In contrast, in the 12-week-old *periostin*$^{-/-}$ mice, lower incisors were shorter than those in the wild-type littermates, and the space between the incisors was wider (Fig. 1B), furthermore, they displayed a chalky white color,

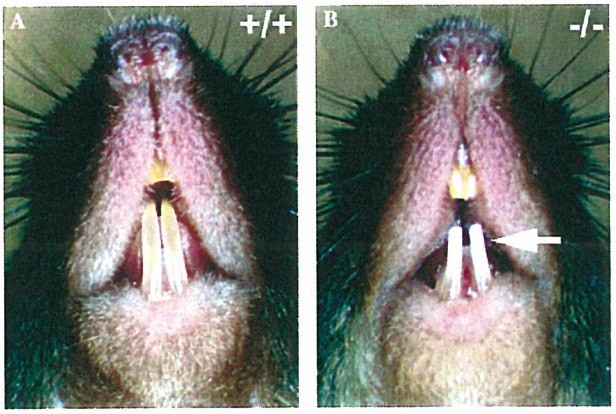

Fig. 1. Abnormal appearance of incisors in the *periostin*$^{-/-}$ mice. Photographs of incisors in 12-week-old wild-type (A) and *periostin*$^{-/-}$ (B) mice. The arrow in (B) indicates short and chalky white incisors in this *periostin*$^{-/-}$ mouse.

indicating disorganization of the enamel layers (Fig. 1B, arrow). Upper incisors of the 12-week-old *periostin*$^{-/-}$ mice also showed similar abnormal phenotypes.

To further investigate whether *periostin* is physiologically involved in eruption of incisors, we cut off one of two lower incisors in the 12-week-old wild-type and the *periostin*$^{-/-}$ mice at the gingival margin, and observed the eruption of incisors 4 days post-operation. In the *periostin*$^{-/-}$ mice, the eruption of the incisor was severely disrupted (Fig. 2B), while in the wild-type mice it normally occurred

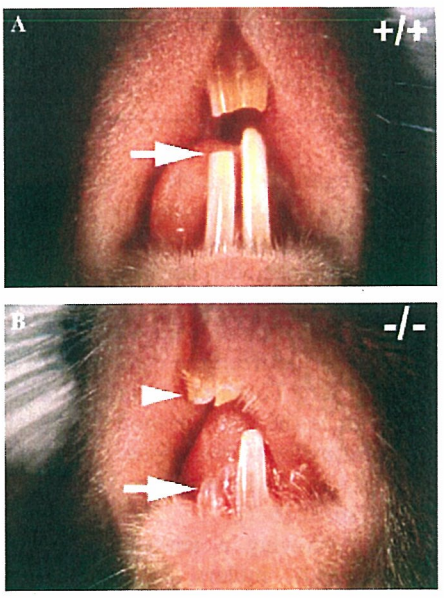

Fig. 2. Eruption disturbance of incisors in the *periostin*$^{-/-}$ mice. Photographs showing incisors that erupted 4-days post-amputation in 12-week-old wild-type (A) and *periostin*$^{-/-}$ (B) mice. In the wild-type mouse, the amputated incisor (left) erupted to the same degree as the intact incisor (right); whereas in the *periostin*$^{-/-}$ animal, the amputated incisor (left) barely erupted. Arrows indicate top of the amputated incisors. Abnormal teeth in the *periostin*$^{-/-}$ mouse are also noted (arrowhead).

(Fig. 2A). These results indicate that periostin acts on the eruption of the incisors.

Disorganization of enamel and dentin layers in the periostin$^{-/-}$ incisors

To investigate the tissue formation in the *periostin*$^{-/-}$ incisors, we performed the histological analyses at the apical region of the incisors. The incisors of rodents are permanently built from the apical bud, and are pushed out anteriorly. In the histological analysis of the apical region in the 6-week-old *periostin*$^{-/-}$ mice, the obvious focal disorganization of ameloblastic layers and the thick dentin and enamel layers, which were waved gently, were observed (Fig. 3B, arrow), compared with those tissues in the wild-type mice (Fig. 3A), although in the *periostin*$^{-/-}$ mice the apical bud generating dental pulp, dentin, and enamel was observed. In the 12-week-old *periostin*$^{-/-}$ mice, the incisal enamel and dentin layers were compressed and undulated (Fig. 3D), though in the wild-type mice they were thin and smooth (Fig. 3C). These findings imply that the incisors in the *periostin*$^{-/-}$ mice became more compressed and undulated from 6- to 12-week-old mice.

In rodents, tooth development, enamel covering of tooth is built in four distinct steps. The first step is the secretion of extracellular matrices and the initiation of enamel crystal growth by polarized ameloblasts (the secretory stage). The second step is the matrix degradation and the differentiation of ameloblasts (the transition stage). The third step is the removal of residual protein components and the crystal growth (the maturation stage). The fourth step is the complete of covering with enamel (the mature stage). These enamel formation processes are found on each incisor of adult mice from the apical region to the front orderly, because of the continuous enamel formation due to the growth and eruption of incisors. High magnification of the ameloblastic layer of the 12-week-old wild-type mice showed a dense cell layer consisting of polarized ameloblasts (nuclei located proximally) in the secretory stage (Fig. 3E), and ameloblasts in the maturation stage (Fig. 3G). In the 12-week-old *periostin*$^{-/-}$ mice, this cell layer was loosened, and partial non-polarized ameloblasts were observed in the secretory stage (Fig. 3F). Moreover, the gaps between the polarized ameloblasts appeared in the maturation stage (Fig. 3H). These histological observations demonstrated that in the *periostin*$^{-/-}$ mice, the morphology and alignment of the ameloblasts were severely disrupted, indicating the impaired enamel layer formation in the absence of *periostin* gene.

The shear zone in the periostin$^{-/-}$ mice

Furthermore, we examined the immunohistological localization of periostin protein at the apical region of the incisors in the 12-week-old wild-type mice. A positive immunoreaction for periostin was observed only in the periodontal ligament of incisors (Fig. 4). At a high magnification, the strong immuno-reactivity for periostin was observed in the middle region of the periodontal ligament corresponding to the shear zone that is the boundary between tooth- and alveolus-related parts (Fig. 4C, arrows), whereas a faint staining was observed in the periodontal ligament close to the cementum and the alveolar bone surface (Fig. 4C). Thus, this strong immuno-reactivity for periostin in the shear zone indicates a role for periostin protein in the shear zone for eruption of the incisors.

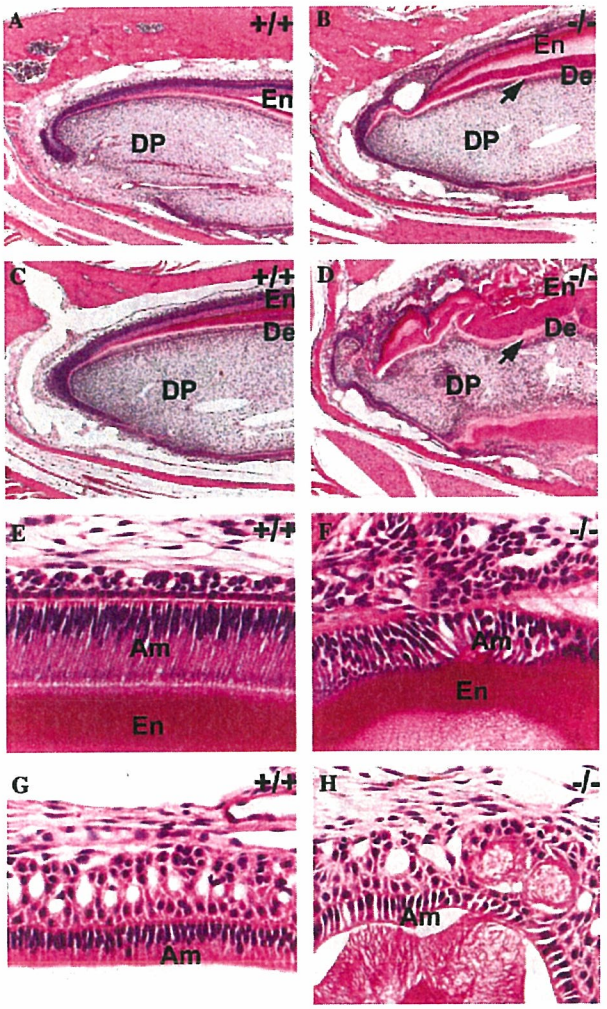

Fig. 3. Histological analysis of the apical region of incisors in the *periostin*$^{-/-}$ mice. Representative histological sections (hematoxylin/eosin stain) of the apical region (root) of incisors in the mandibles from 6-week- (A,B) and 12-week- (C,D) old wild-type (+/+) and *periostin*$^{-/-}$ (−/−) mice show that incisal enamel and dentin are compressed and undulated in the *periostin*$^{-/-}$ mice (arrows). Histological sections (hematoxylin/eosin staining) at high magnifications of the secretory stage (E,F) and the maturation stage (G,H) of enamel in 12-week-old wild-type (+/+) and *periostin*$^{-/-}$ (−/−) mice show disorganized enamel layers in the *periostin*$^{-/-}$ mice. DP, dental pulp; En, enamel; De, dentin; Am, ameloblastic layer.

To address the requirement for periostin protein in the shear zone, we histologically analyzed sections of the periodontal ligament around the incisors in the *periostin*$^{-/-}$ mice. The shear zone was clearly distinguishable

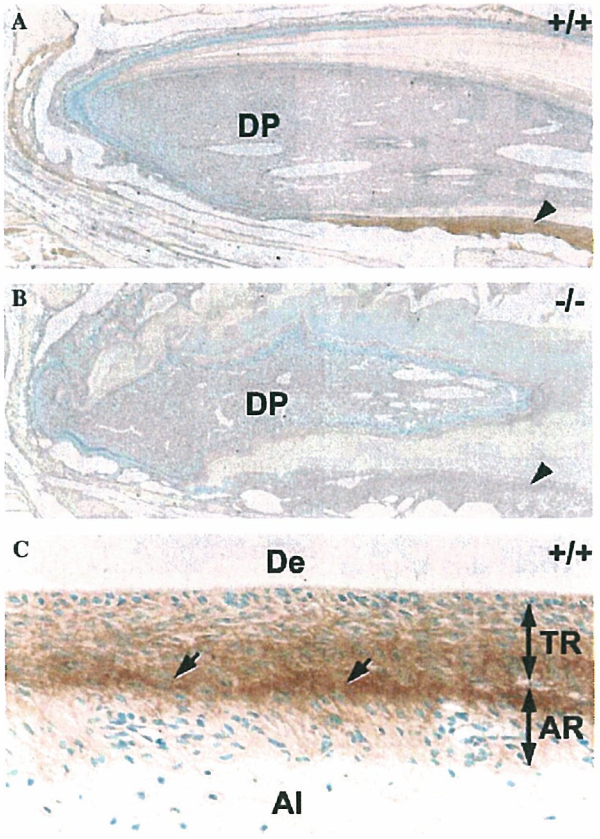

Fig. 4. Immunohistological localization of periostin protein in the periodontal ligament. Immuno-localization of periostin in the periodontal ligament of incisors (A,C) from 12-week-old wild-type (A,C) and *periostin*$^{-/-}$(B) mice. The specific immunoreactivity for periostin is seen in the wild-type periodontal ligament (A, arrowhead), whereas *periostin*$^{-/-}$ mice have no expression of periostin protein there at all (B, arrowhead). Arrows in (C) indicate the shear zone, which is the boundary between the TR (tooth-related) and AR (alveolus-related) regions. Strong immunoreactivity for periostin is observed in the shear zone of the incisor periodontal ligament. DP, dental pulp; De, dentin; Al, alveolar bone.

in hematoxylin and eosin-stained sections from both the control 6- and the 12-week-old wild-type mice, and it appeared as a line when observed by microscopy (Figs. 5A and C, arrows). In the 6-week-old *periostin*$^{-/-}$ mice, the line in the shear zone was obscure (Fig. 5B). Notably, in the 12-week-old *periostin*$^{-/-}$ mice, the shear zone was completely disappeared, and the periodontal ligament was wider than that of the wild-type mice (Fig. 5D).

To examine the ultrastructure of the shear zone in the *periostin*$^{-/-}$ mice, we carried out electron-microscopic examination of the periodontal ligament around the incisors. In the 12-week-old wild-type mice, we observed the presence of fragmented collagen fibrils extracellularly (Fig. 5E), suggesting digestion of collagen fibrils in the shear zone. In contrast, in the *periostin*$^{-/-}$ mice, abundant intact collagen fibrils occupied the shear zone, and the line disappeared (Fig. 5F). These results suggest that *periostin* is required for the digestion process of collagen fibrils in the shear zone.

Periostin protein localized to collagen fibrils

To understand the molecular mechanism leading to formation of the shear zone, we focused on the extracellular matrix localization of periostin protein, because periostin is known to be localized in the boundary between the cells and extracellular matrix [12–14].

To investigate the extracellular matrix localization of periostin in the periodontal ligament in vivo, we conducted immuno-electron microscopic analysis using anti-periostin antibodies. Our results showed that the immuno-reactivity was detected mainly on the extracellular collagen fibrils, suggesting a possible interaction between periostin protein and collagen fibrils (Figs. 6A and B).

Discussion

In this study based on observations on *periostin*$^{-/-}$ mice, we show that *periostin* is required for formation of the shear zone in the periodontal ligament of incisors. Although several MMPs are involved in remodeling of the periodontal ligament in the previous studies [3–7], the molecular biological aspect of the shear zone is not studied well. The present study showed that periostin protein localized to the shear zone and interacted to the collagen fibrils. Since it was reported that remodeling of collagens predominantly occurs in the shear zone [9], our findings suggest that periostin protein plays a role in remodeling of collagen matrix.

Our electron microscopic analysis in the wild-type mice demonstrated that the digestion of collagen fibers occurred in the shear zone, suggesting that digestion of collagen fibers in this zone may be necessary for an appropriate eruption of incisors. However, in the *periostin*$^{-/-}$ mice, the same observation showed existence of abundant collagen fibers in the intercellular spaces and few digested ones compared with the wild-type littermates. The collagen fibers detected in the periodontal ligament of the *periostin*$^{-/-}$ mice appeared to connect the cementum to the alveolar bone tightly. This tight connection may have prevented the eruption of incisors in the *periostin*$^{-/-}$ mice.

In the *periostin*$^{-/-}$ mice, the defective remodeling in the periodontal ligament of the incisors became more severe as the animals aged. This observation indicates that no remodeled and metabolized extracellular matrices are accumulated to form an abnormal ligament as the animals aged in the absence of *periostin*.

Because disruption of the *periostin* gene caused the accumulation of undigested collagen fibers, periostin may be connected with the digestion of collagen fibers in the shear zone. In the shear zone, the movement between the tooth- and alveolus-related parts causes mechanical stress, and periodontal fibroblasts must sense and respond to this stress. In previous reports, expression of periostin was increased under the mechanically stressful condition of orthodontic tooth movement [17], and decreased by occlusal hypofunction in the mouse periodontal ligament [18].

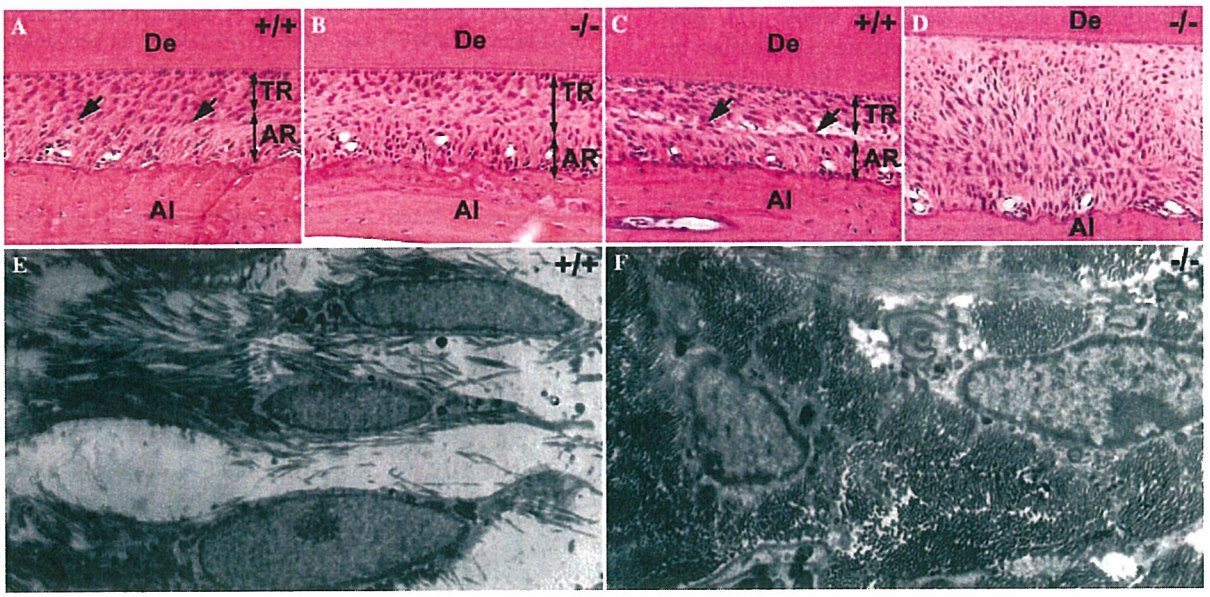

Fig. 5. Remodeling of the periodontal ligament of incisors is defective in periostin$^{-/-}$ mice. Histological micrographs (hematoxylin/eosin staining) of the periodontal ligament from 6-week- (A,B) and 12-week- (C,D) old wild-type (+/+) and periostin$^{-/-}$ (−/−) mice. Arrows indicate the shear zone, which is the boundary between the TR (tooth-related) and AR (alveolus-related) regions. The shear zone in wild-type mice (A,C) is clearly distinguishable, whereas it is obscure in 6-week-old periostin$^{-/-}$ mice (B) and is completely absent in 12-week-old periostin$^{-/-}$ mice (D). Electron microscopy of the incisor periodontal ligament shows evidence of digestion of collagen fibers in 12-week-old wild-type mice (E), but undigested and abundant collagen bundles in 12-week-old periostin$^{-/-}$ mice (F). DP, dental pulp; En, enamel; De, dentin; Al, alveolar bone; TR, tooth-related region; and AR, alveolus-related region.

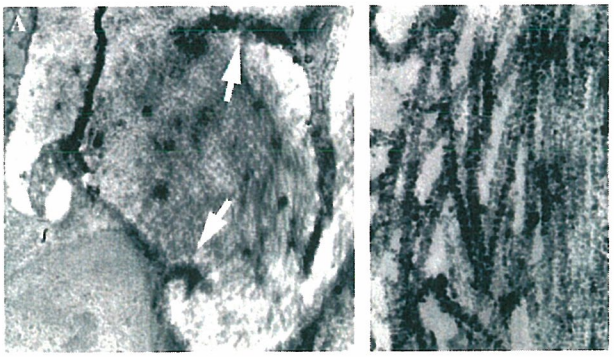

Fig. 6. Immuno-electron microscopic analysis for periostin. Immunoreactivity for periostin is observed in the boundary between cells and the extracellular matrix in the periodontal ligament of the wild-type mice (A, arrows). At a high magnification of the collagen fibers, periostin is seen to be associated with the collagen fibers (B).

These results indicate that in the shear zone, mechanical stress caused by the movement of tooth-related parts may increase the expression of periostin in the shear zone.

The *periostin*$^{-/-}$ mice showed abnormal appearance of incisors, especially disorganized enamel layers and compressed and undulated dentin layers. The present study demonstrates the specific function of periostin in the shear zone. We concluded that the incisors of the *periostin*$^{-/-}$ mice were continuously built in the apical region, but could not erupt because of the defective remodeling of the periodontal ligament, therefore, demonstrating the compressed appearance of the enamel and dentin of their incisors.

However, there is one question whether *periostin* is involved in formation of the enamel and dentin, and affects the functions of the ameloblast and odontoblast directly. In the ameloblastic layer and the apical bud, expression of periostin is barely observed. Periostin localized to the periodontal ligament specifically in the incisors of mice, suggesting that the function of periostin may be restricted to the periodontal ligament.

Our recent findings indicate that periostin protein binds directly to type I collagen in vitro (Shimazaki et al., manuscript in preparation). Periostin protein in the periodontal ligament was associated with the collagen fibers in vivo. These results suggest that periostin protein in vivo binds to type I collagen fibers directly. Periostin is a member of the fasciclin I family, whose members include β ig-h3 protein [10]. It has been reported that β ig-h3 also binds to collagens directly [19,20]. Our results and these previous reports suggest a common function between periostin and β ig-h3 proteins. Furthermore, periostin acts as a cell spreading factor for fibroblastic cells [12,21] and is reported as a ligand for integrin αVβ3 or αVβ5 [21–23]; and its four Fas I domains are postulated to be a binding domain for integrin from the results of biochemical analysis of β ig-h3 [24,25]. These findings imply the existence of a collagen–periostin–integrin complex in the shear zone.

Periostin is a highly conserved protein among various species such as human, dog, rat, mouse, chick, and zebrafish (data not shown). Zebrafish periostin is required for formation of the myoseptum, which is composed of dense collagens [26]. The myoseptum is a connective tissue

layer that divides the somites from the trunk [27]. The structure and function of the myoseptum are similar to those of the mammalian tendon. Both the myoseptum and tendon serve as the transmitter of muscular contractility to bones and adjoining muscles, and their structures are indispensable for movement of vertebrate animals. The tendon is also composed of dense collagen fibers, and is exposed to mechanical stress caused by physical exercise, just as are the periodontal ligament and the periosteum [28,29]. Furthermore, expression of mouse periostin is also found in tendons [13]. Tissues that are exposed to strong mechanical stress form a dense collagenous extracellular matrix, and this matrix is remodeled sufficiently to tolerate the stress when the tissues are deformed by strong mechanical stress beyond the permissible range. These previous findings and our present results suggest that periostin is responsible for triggering the remodeling of collagenous tissues.

To our knowledge, this is the first report on a molecule responsible for formation of the shear zone. The periodontal ligament in humans is also responsible for the eruption and realignment of teeth. The *periostin* is a gene whose sequence is highly conserved between mice and humans [10], and periostin protein was also detected in the human periodontal ligament (unpublished results). Therefore, *periostin*$^{-/-}$ mice provide a novel model system to evaluate the cause of eruption disturbance and malocclusion in humans.

Acknowledgments

We thank A. Moriyama, Y. Nakatani, and M. Shimazaki for critical reading of the manuscript; E. Ikeno for technical assistance in the generation of *periostin*$^{-/-}$ mice; Y. Hattori for technical assistance in protein purification; M. Ikumi, T. Nishiyama, Y. Nagano, and K. Kume for the maintenance and manipulation of the animals; H. Tanabe, A. Oshima, and K. Horiuchi for their technical advice. This work was supported by grants from the Promotion of Niigata University Research Project and from the Ministry of Education, Sports, Science and Technology.

References

[1] P. Lekic, J. Rojas, C. Birek, H. Tenenbaum, C.A. McCulloch, Phenotypic comparison of periodontal ligament cells in vivo and in vitro, J. Periodontal Res. 36 (2001) 71–79.

[2] B.K. Berkovitz, Periodontal ligament: structural and clinical correlates, Dent. Update 31 (2004) 46–50, pp. 52, 54.

[3] V. Everts, E. van der Zee, L. Creemers, W. Beertsen, Phagocytosis and intracellular digestion of collagen, its role in turnover and remodelling, Histochem. J. 28 (1996) 229–245.

[4] M.T. van der Pauw, T. Van den Bos, V. Everts, W. Beertsen, Phagocytosis of fibronectin and collagens type I, III, and V by human gingival and periodontal ligament fibroblasts in vitro, J. Periodontol. 72 (2001) 1340–1347.

[5] I. Takahashi, M. Nishimura, K. Onodera, J.W. Bae, H. Mitani, M. Okazaki, Y. Sasano, Expression of MMP-8 and MMP-13 genes in the periodontal ligament during tooth movement in rats, J. Dent. Res. 82 (2003) 646–651.

[6] M. Tsubota, Y. Sasano, I. Takahashi, M. Kagayama, H. Shimauchi, Expression of MMP-8 and MMP-13 mRNAs in rat periodontium during tooth eruption, J. Dent. Res. 81 (2002) 673–678.

[7] A.L. Bolcato-Bellemin, R. Elkaim, A. Abehsera, J.L. Fausser, Y. Haikel, H. Tenenbaum, Expression of mRNAs encoding for alpha and beta integrin subunits, MMPs, and TIMPs in stretched human periodontal ligament and gingival fibroblasts, J. Dent. Res. 79 (2000) 1712–1716.

[8] W. Beertsen, V. Everts, A. van den Hooff, Fine structure and possible function of cells containing leptomergic organelles in the periodontal ligament of the rat incisor, Arch. Oral Biol. 19 (1974) 1099–1100.

[9] W. Beertsen, V. Everts, The site of remodeling of collagen in the periodontal ligament of the mouse incisor, Anat. Rec. 189 (1977) 479–497.

[10] S. Takeshita, R. Kikuno, K. Tezuka, E. Amann, Osteoblast-specific factor 2: cloning of a putative bone adhesion protein with homology with the insect protein fasciclin I, Biochem. J. 294 (Pt. 1) (1993) 271–278.

[11] T. Sugiura, H. Takamatsu, A. Kudo, E. Amann, Expression and characterization of murine osteoblast-specific factor 2 (OSF-2) in a baculovirus expression system, Protein Expr. Purif. 6 (1995) 305–311.

[12] K. Horiuchi, N. Amizuka, S. Takeshita, H. Takamatsu, M. Katsuura, H. Ozawa, Y. Toyama, L.F. Bonewald, A. Kudo, Identification and characterization of a novel protein, periostin, with restricted expression to periosteum and periodontal ligament and increased expression by transforming growth factor beta, J. Bone Miner. Res. 14 (1999) 1239–1249.

[13] Y. Hirose, H. Suzuki, N. Amizuka, J. Shimomura, Y. Kawano, K. Nozawa-Inoue, A. Kudo, T. Maeda, Immunohistochemical localization of periostin in developing long bones of mice, Biomed. Res. 24 (2003) 31–37.

[14] H. Suzuki, N. Amizuka, I. Kii, Y. Kawano, K. Nozawa-Inoue, A. Suzuki, H. Yoshie, A. Kudo, T. Maeda, Immunohistochemical localization of periostin in tooth and its surrounding tissues in mouse mandibles during development, Anat. Rec. (2004).

[15] I. Kii, N. Amizuka, S. Kitajima, M. Li, K. Takeuchi, T. Maeda, J. Kanno, T. Inoue, Y. Saga, A. Kudo, Mechanical stress dependent remodeling of the periodontal ligament is defective in periostin deficient mice: mechanotransduction through periostin protein, J. Bone Miner. Res. 19 (Suppl. 1) (2004) s21.

[16] N. Amizuka, H.S. Lee, M.Y. Kwan, A. Arazani, H. Warshawsky, G.N. Hendy, H. Ozawa, J.H. White, D. Goltzman, Cell-specific expression of the parathyroid hormone (PTH)/PTH-related peptide receptor gene in kidney from kidney-specific and ubiquitous promoters, Endocrinology 138 (1997) 469–481.

[17] J. Wilde, M. Yokozeki, K. Terai, A. Kudo, K. Moriyama, The divergent expression of periostin mRNA in the periodontal ligament during experimental tooth movement, Cell Tissue Res. 312 (2003) 345–351.

[18] E. Afanador, M. Yokozeki, Y. Oba, Y. Kitase, T. Takahashi, A. Kudo, K. Moriyama, Messenger RNA expression of periostin and Twist transiently decrease by occlusal hypofunction in mouse periodontal ligament, Arch. Oral Biol. 50 (2005) 1023–1031.

[19] E. Hanssen, B. Reinboth, M.A. Gibson, Covalent and non-covalent interactions of betaig-h3 with collagen VI. Beta ig-h3 is covalently attached to the amino-terminal region of collagen VI in tissue microfibrils, J. Biol. Chem. 278 (2003) 24334–24341.

[20] K. Hashimoto, M. Noshiro, S. Ohno, T. Kawamoto, H. Satakeda, Y. Akagawa, K. Nakashima, A. Okimura, H. Ishida, T. Okamoto, H. Pan, M. Shen, W. Yan, Y. Kato, Characterization of a cartilage-derived 66-kDa protein (RGD-CAP/beta ig-h3) that binds to collagen, Biochim. Biophys. Acta 1355 (1997) 303–314.

[21] L. Gillan, D. Matei, D.A. Fishman, C.S. Gerbin, B.Y. Karlan, D.D. Chang, Periostin secreted by epithelial ovarian carcinoma is a ligand for alpha(V)beta(3) and alpha(V)beta(5) integrins and promotes cell motility, Cancer Res. 62 (2002) 5358–5364.

[22] R. Shao, S. Bao, X. Bai, C. Blanchette, R.M. Anderson, T. Dang, M.L. Gishizky, J.R. Marks, X.F. Wang, Acquired expression of periostin by human breast cancers promotes tumor angiogenesis through up-regulation of vascular endothelial growth factor receptor 2 expression, Mol. Cell. Biol. 24 (2004) 3992–4003.
[23] S. Bao, G. Ouyang, X. Bai, Z. Huang, C. Ma, M. Liu, R. Shao, R.M. Anderson, J.N. Rich, X.F. Wang, Periostin potently promotes metastatic growth of colon cancer by augmenting cell survival via the Akt/PKB pathway, Cancer Cell 5 (2004) 329–339.
[24] J.E. Kim, S.J. Kim, B.H. Lee, R.W. Park, K.S. Kim, I.S. Kim, Identification of motifs for cell adhesion within the repeated domains of transforming growth factor-beta-induced gene, betaig-h3, J. Biol. Chem. 275 (2000) 30907–30915.
[25] J.E. Kim, H.W. Jeong, J.O. Nam, B.H. Lee, J.Y. Choi, R.W. Park, J.Y. Park, I.S. Kim, Identification of motifs in the fasciclin domains of the transforming growth factor-beta-induced matrix protein betaig-h3 that interact with the alphavbeta5 integrin, J. Biol. Chem. 277 (2002) 46159–46165.
[26] H. Kudo, N. Amizuka, K. Araki, K. Inohaya, A. Kudo, Zebrafish periostin is required for the adhesion of muscle fiber bundles to the myoseptum and for the differentiation of muscle fibers, Dev. Biol. 267 (2004) 473–487.
[27] G.M. Dubois, Z. Haftek, C. Crozet, R. Garrone, D. Le Guellec, Structure and spatio temporal expression of the full length DNA complementary to RNA coding for alpha2 type I collagen of zebrafish, Gene 294 (2002) 55–65.
[28] A.P. Summers, T.J. Koob, The evolution of tendon–morphology and material properties, Comp. Biochem. Physiol. A Mol. Integr. Physiol. 133 (2002) 1159–1170.
[29] T.J. Koob, A.P. Summers, Tendon–bridging the gap, Comp. Biochem. Physiol. A Mol. Integr. Physiol. 133 (2002) 905–909.

ELSEVIER

EXPERIMENTAL HEMATOLOGY

Experimental Hematology 34 (2006) 1687–1697

Thioredoxin overexpression in mice, model of attenuation of oxidative stress, prevents benzene-induced hemato-lymphoid toxicity and thymic lymphoma

Guang-Xun Li[a,†], Yoko Hirabayashi[a,†], Byung-Il Yoon[a,*], Yasushi Kawasaki[a], Isao Tsuboi[a], Yukio Kodama[a], Yuji Kurokawa[a], Junji Yodoi[b], Jun Kanno[a], and Tohru Inoue[c]

[a]*Division of Cellular and Molecular Toxicology, Biological Safety and Research Center, National Institute of Health Sciences, Tokyo, Japan;* [b]*Department of Biological Responses, Research Center for Immunodeficiency Virus, Institute for Virus Research, Kyoto University, Kyoto, Japan;* [c]*Biological Safety and Research Center, National Institute of Health Sciences, Tokyo, Japan*

(Received 6 March 2006; revised 10 July 2006; accepted 9 August 2006)

Objective. **Reactive oxygen species (ROS), generated following benzene exposure, are considered to trigger the development of hematopoietic neoplasms, although little supporting evidence has been found. In this study, we examined whether the experimental elimination of ROS generated following benzene exposure prevents the development of benzene-induced hematopoietic disorders to clarify the mechanism underlying the development of benzene-induced hematopoietic disorders.**

Methods. **C57BL/6 mice, overexpressing human thioredoxin (h-Trx-Tg), were used to examine the possible nullification of ROS induction following benzene exposure. The experimental group was exposed to 300 ppm benzene 6 hours/day, 5 days/week, for 26 weeks, and lifetime observation followed by molecular and histopathological examinations were carried out.**

Results. **The present study using h-Trx-Tg mice showed a complete suppression of the development of thymic lymphoma induced by benzene inhalation (0% in h-Trx-Tg vs 30% in wild-type (Wt) mice). This was associated with a 48% decrease in the incidence of clastogenic micronucleated reticulocyte induction in the h-Trx-Tg mice compared with the Wt control after 2 weeks of inhalation. As underlying mechanisms, the attenuation of oxidative stress was accompanied by a complete abrogation of hemato-lymphoid toxicity, as shown by the upregulation of the activity of superoxide-dismutase, and a consequently stable ROS level, as determined by cell sorting using 2′, 7′-dichlorodihydrofluorescein diacetate, along with a significant attenuation of the overexpression of a cell cycle–dependent kinase inhibitor, p21.**

Conclusion. **The attenuation of benzene-induced oxidative stress and that of the consequent lymphomagenesis were observed for the first time, and these indicate a role of oxidative stress in benzene-induced clastogenesis and lymphomagenesis. (These attenuations were not seen in nonthymic lymphomas, and no leukemias developed in C57BL/6 used in this study.) During the constitutive overexpression of h-*Trx*, the expression of aryl-hydrocarbon receptor in h-Trx-Tg mice was downregulated, which may also contribute to the attenuation.** © **2006 International Society for Experimental Hematology. Published by Elsevier Inc.**

Benzene, a ubiquitous contaminant in the environment, is a volatile solvent released from petroleum products such as natural gas condensates or industrial intermediates [1], as well as from vehicular emissions [2] and cigarette smoke [3]. Epidemiological studies such as those of shoe workers are still the focus of much interest [4,5], and the impact of benzene at levels below the U.S. occupational standard of 1 part per million (ppm) makes risk characterization problematic [6]. Phenolic metabolites derived from cytochrome p450 2E1 (CYP2E1) rearranged via benzene oxide [7] are

Offprint requests to: Yoko Hirabayashi, M.D., Ph.D., Cellular and Molecular Toxicology Division, Center for Biological Safety and Research, National Institute of Health Sciences, 1-18-1 Kamiyohga, Setagayaku, Tokyo 158-8501, Japan; E-mail: yokohira@nihs.go.jp

*Present address: Department of Veterinary Medicine, College of Animal Resource, Kangwon National University, Kangwon-Do 200-701, Republic of Korea.

†Guang-Xun Li and Yoko Hirabayashi both contributed equally to this work.

0301-472X/06 $–see front matter.
doi: 10.1016/j.exphem.2006.08.005

considered to be generators of reactive oxygen species (ROS) after hydroxylation by myeloperoxidase, and the consequent oxidative stresses are further considered to induce acute hemato-lymphoid toxicity in the bone marrow (BM) [8,9]. However, the mechanism underlying lympho/leukemogenicity remains unclarified, because the Ames revertant mutagenesis assay of benzene and its major metabolites is known to yield negative results [10,11] and neither sufficient DNA binding nor a significant amount of adduct formation is observed [12,13], probably owing to the less electrophilic nature of benzene and its metabolites [14]. Hence, previous studies on the induction of ROS during benzene metabolism only focused on other types of genotoxic damage. Other types of chromosomal damage including clastogenic micronucleic reticulocyte formation [15] induced by ROS and benzene and its metabolites, namely, hydroquinone, catechol, and *trans-trans*-muconic acid, are assumed to be the consequences of genotoxicities [16]. This may be in good agreement with the observed severe benzene toxicity in p53-knockout (KO) mice. However, there has been no direct in vivo evidence, and only a few in vitro studies indicating that an increase in the rate of homologous recombination initiated by benzene monoxide induces oxidative stress have been reported [17]. Because thioredoxin (Trx) might protect mice against oxidative stress following benzene exposure, genetically modified Trx mice, specifically transgenic Trx mice, were used to support the above-mentioned contention.

Genetically modified mice, namely Trx-KO mice and Trx-overexpressing (Tg) mice, respond to ROS in a *Trx* gene-dosage-dependent manner. Human (h) Trx-Tg mice were used in the present study to resolve the above controversy, because h-Trx-Tg mice are tolerant to oxidative stress [18–20] and may elucidate whether oxidative stress is a major trigger of benzene-induced hematopoietic neoplasms in vivo. The exacerbation of benzene-induced hemato-lymphoid toxicity in Trx-KO ($Trx^{+/-}$) mice and the attenuation of that in h-Trx-Tg mice confirm, for the first time, that the hemato-lymphoid toxicity is caused by oxidative stress at the whole-animal level. Furthermore, although nonthymic lymphoma was not suppressed, benzene-induced thymic lymphomagenesis was inhibited 100% in h-Trx-Tg mice, and the mechanism underlying benzene-induced lymphomagenesis was also elucidated to involve oxidative stress.

Materials and methods

Experimental animals

h-Trx-Tg, $Trx^{+/-}$, and wild-type (Wt) mice were maintained in the board-approved laboratory animal facility of the National Institute of Health Sciences (NIHS) of Japan. The h-Trx-Tg and Trx-KO C57BL/6 mice were originally bioengineered by Mitsui et al. [19] and Matsui et al. [21], respectively. Because the homozygousity for Trx KO is embryonic lethal, $Trx^{+/-}$ mice were used in this study. Both $Trx^{+/-}$ mice and h-Trx-Tg mice were maintained in heterozygosity and their genotypes were confirmed at the weaning stage by the polymerase chain reaction (PCR) screening of DNA from the tail of each mouse. The expression levels of the endogenous murine (m)*Trx* gene, during the steady state of Wt mice, h-Trx-Tg mice, and $Trx^{+/-}$ mice, three of each, used in the present study are shown in Figure 1. In the $Trx^{+/-}$ mice, because the mice are Trx hemizygous KO, the m-*Trx* expression level was nearly one-half in allelic number that in Wt mice, whereas h-Trx-Tg mice showed the same expression level as that in Wt steady-state mice.

Benzene

Benzene, Cas. No. 71-43-2, MW 78.11, was purchased from Wako Fine Chemical Company (Osaka, Japan).

Benzene exposure and dose monitoring

The mice were randomly assigned to groups and individually housed. They were exposed to benzene in 1.3m^3 inhalation chambers as described previously [22,23]. Briefly, benzene vapor was generated by heating liquid benzene to 16°C and directed into the inhalation chambers (Sibata Scientific Technology Ltd., Tokyo, Japan). The flow rate of benzene was about 650 L/min, and benzene concentration in the chambers was measured at 30-minute intervals during daily exposures using a gas chromatograph (Shimadzu Co., Kyoto, Japan). The temperature and humidity in the chambers were automatically controlled at 24°C ± 1°C and 55% ± 10%, respectively. The incoming air and exhaust air were passed through high-efficiency particulate-air filters.

For short-term exposure, the mice were divided into sham-exposed and benzene-exposed groups. Benzene was exposed to 300 ppm for 6 hours/day, 5 days/week for 2 weeks. The sham-exposed mice were maintained under the same conditions as the benzene-exposed group except for benzene inhalation.

For long-term exposure in the lymphomagenicity study, see later sections.

Peripheral blood parameters and BM cellularity

Peripheral blood from three mice of each genotype was collected from the orbital plexus, and blood parameters were measured using a Sysmex M-2000 blood cell counter (Sysmex Co., Osaka,

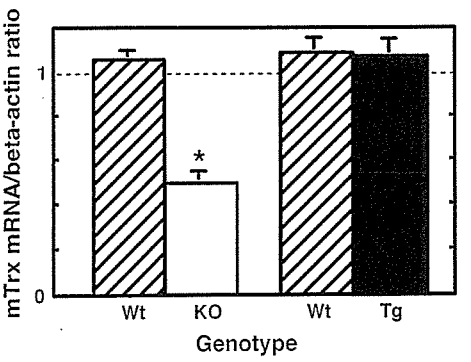

Figure 1. Steady-state murine (m)-*Trx* gene expressions of BM cells from three mice of each of endogenous $Trx^{+/-}$ (open column) and h-Trx-Tg mice (closed column), compared with those in littermate Wt mice (each paired hatched column). The ordinate (y axis) indicates the ratio of mRNA expression level of m-Trx to that of β-actin (*: $p < 0.05$).

Japan). BM cells from bilateral femurs of three mice of each genotype were harvested from the benzene-exposed and sham-exposed mice. Total and differential cell counts were also determined using a Sysmex M-2000.

In vitro colony assays

Colony-forming unit granulocyte-macrophages (CFU-GMs) were assayed in a semisolid methylcellulose culture medium [23,24]. Briefly, a mixture of 8×10^4 BM cells from three mice of each genotype were suspended in 4 mL of α-medium containing 0.8% methylcellulose (Nakalai Tesque, Co., Ltd., Kyoto, Japan), 30% fetal calf serum (HyClone Laboratories, Inc., Logan, UT, USA), 1% bovine serum albumin (Sigma, St. Louis, MO, USA), 10^{-4} M 2-mercaptoethanol (Sigma), and 10 ng/mL murine granulocyte-macrophage colony-stimulating factor (m-GM-CSF, R&D Systems, Inc., Minneapolis, MN, USA). One milliliter of methylcellulose medium containing this cell suspension was plated in 35-mm tissue culture wells in triplicate (Nalgen Nunc International, Naperville, IL, USA) and incubated in a humidified chamber at 37°C in 5% CO_2 for 6 days. Colonies were counted under an inverted microscope (Olympus, Tokyo, Japan).

Micronucleus analysis of peripheral blood

Acridine orange (AO)-coated glass slides (Toyobo, Kyoto, Japan) and peripheral blood cells were prepared as described previously [25]. A blood sample collected from the same three mice of each genotype at each time point (i.e., before and 3, 5, 10, 12, 15, and 18 days after benzene inhalation) was placed at the center of an AO-coated glass slide and covered with a 24 × 40-mm cover slip. Supravitally AO-stained reticulocytes were examined under a fluorescence microscope with a blue excitation filter and a yellow barrier filter. The frequency of micronucleated reticulocytes (MN-Rets) among 2000 cells per mouse was determined.

Assay of benzene-induced lymphomagenicity

For lymphomagenicity studies, the numbers of mice per groups, namely, Wt mice with or without benzene exposure, and Tg mice with or without benzene exposure, were 10 BWt mice, 8 CWt mice, 13 BTg mice, and 8 CTg mice, respectively. The mice were supplied water ad libitum, but food pellets were withdrawn during the exposure. For long-term exposure, the mice were divided into the sham-exposed control and the benzene-exposed groups. The latter group was exposed to 300 ppm benzene 6 hours/day, 5 days/week, for 26 weeks. The sham-exposed control group was maintained under the same conditions as the benzene-exposed group except for benzene inhalation. All the mice were monitored throughout their lifetime except for those showing symptoms of advanced hematopoietic neoplasms such as anemia and palpable splenomegaly; these were euthanized at the agonal period and then examined hematopathologically. The remaining mice were also examined histopathologically.

Histopathological examination

For the evaluation of hemopoietic malignancies caused by benzene inhalation in Wt and h-Trx-Tg mice, mice from each group were sacrificed under ethyl ether anesthesia for autopsy. For the histopathological examination, all the visceral organs including the thymus, spleen, sternum, and femoral BM were fixed in 10% neutral buffered formalin for 24 hours. The sternum and femoral BM were decalcified in 7.5% formic acid for 72 hours. After conventional processing, paraffin-embedded sections were stained with hematoxylin and eosin (H & E) and then examined histopathologically under a light microscope. The diagnostic definition of histopathological typing for lymphomagenesis was according to previous publications [26,27].

Reverse transcription and polymerase chain reaction

The expression of genes encoding murine and human Trx, $p21^{waf1}$, aryl hydrocarbon receptor (AhR), and CYP2E1 was evaluated by reverse transcription (RT) followed by a PCR technique. Total RNA from the BM cells of three mice of each genotype at each time point was isolated using a Qiagen RNAeasy kit (Qiagen, Valencia, CA, USA).

RT was performed using total RNA and random hexamers as primers with a reverse transcription kit from Applied Biosystems (Foster City, CA, USA). PCR amplification was performed using the following previously designed oligonucleotide primers [28]: For mouse AhR, forward primer 5′-GAT GCC TTG GTC TTC TAT-3′, reverse primer 5′-TCATGCCACTTTCTCCAGTCT-3′; for mouse $p21^{waf1}$, forward primer 5′-ATCTCCAATCCTGGT-GATGT-3′, reverse primer 5′-TGCAGCAGGGCAGAGGAAGT-3′; for mouse CYP2E1, forward primer 5′-TGACTTTGGCCGA CCTGTTC-3′, reverse primer 5′-GAATCAGGAGCCCATATCT-3′.

The expression of murine and human Trx mRNAs was also quantitatively evaluated by real-time PCR using TaqMan with the Applied Biosystems 7900HT Sequence Detection System (Applied Biosystems). PCR conditions and data analysis were according to SDS ver.2.0. All of the samples were run in triplicate using the *glyceraldehyde-3-phosphate dehydrogenase* (*GAPDH*) gene as the standard gene, because *GAPDH* expression level does not change significantly across genotypes or with benzene exposure time, as shown in Figures 3, 7, and 10. For the quantitative evaluation of mRNA expression, the following four primers and corresponding probes were designed using computer software Primer Express ver. 1.5 (Applied Biosystems): For m-Trx mRNA, forward primer 5′-GGATGTTGCTGCAGACTGTGA-3′, reverse primer 5′-CCCCACCTTTTGACCCTTTT-3′, the probe 5′-FAM-TCAAATGCATGCCGACCTTCCAGTT-TAMRA-3′; for h-Trx mRNA, forward primer 5′-CCATTTCCATCGGTCCTTACA-3′, reverse primer 5′-GCTCTCGATCTGCTTCACCAT-3′, the probe 5′-FAM-CGCTCGTCAGACTCCAGCAGCCA-TAMRA-3′; for m-β-actin, forward primer 5′-GCTCTGGCTCCTAGCACCAT-3′, reverse primer 5′-GCCACCGATCCACACAGAGT-3′, the probe 5′-VIC-CAAGATCATTGCTCCTCCTGAGCGCA-TAMRA-3′; for m-GAPDH, forward primer 5′-TGTGTCCGTCGTGGATCTGA-3′, reverse primer 5′-CCTGCTTCACCACCTTCTTGA-3′, the probe 5′-VIC-CCGCCTGGAGAAACCTGCCAAGTATG-TAMRA-3′.

Western blot analysis

Total protein (15 μg) from BM cells of three mice of each genotype was electrophoresed in a 15% SDS-polyacrylamide gel. Separated proteins were transferred to a nitrocellulose membrane (Hybond-ECL; Amersham, Arlington Heights, IL, USA). The p21 protein was visualized by immunostaining with a rabbit anti-mouse p21 polyclonal antibody (Santa Cruz Biotechnology, Inc., Santa Cruz, CA, USA) and an anti-rabbit-HRP-conjugated anti-rabbit p21 polyclonal antibody (Santa Cruz Biotechnology) in ECL detection reagent (ECL, RPN 2209) (Amersham Life Science, CA, USA).

Assay of superoxide dismutase activity of BM

The total Cu/Zn and Mn superoxide dismutase (SOD) activity was determined essentially using the method described by Fridovich [29]. An SOD assay kit (Wako, Osaka, Japan) was used for the quantification of total SOD activity. SOD activity was determined from the percentage inhibition of xanthine-xanthine oxidase-reduced nitroblue tetrazolium (NTB). Briefly, BM cells from three mice of each genotype were lysed in 0.1% Triton X, subjected to two freeze/rethaw cycles, and then stored on ice. The increase in absorbance at 560 nm was monitored at 37°C for 20 minutes using a spectrophotometer (Beckman DU-600, Beckman Coulter, Inc., Fullerton, CA, USA).

Measurement of erythrocyte ROS production

In the assessment of the attenuation of benzene-induced ROS production in the h-Trx-Tg mice, we loaded erythrocytes from the same three mice of each genotype at each time point with a 20-μM fluorescent probe, 2′,7′-dichlorodihydrofluorescein diacetate (DCFH-DA, Sigma, St. Louis, MO, USA), and analyzed intracellular fluorescence intensity by flow cytometry [30–32]. Briefly, peripheral blood (5 μL) was obtained from the mouse tail. Blood was washed once and diluted with Ca^{2+}- and Mg^{2+}-free Dulbecco's phosphate-buffered saline (D-PBS) (Invitrogen Corp., Carlsbad, CA, USA) to a concentration of 1×10^6 cells/mL. To this preparation, 20 μM DCFH-DA dye was added after incubation at 37°C for 15 minutes in a humidified atmosphere of 5% CO_2. The obtained red blood cell (RBC) suspension was washed with D-PBS. RBCs were obtained using a fluorescence-activated cell sorter (FACS-Calibur, Becton-Dickinson, San Francisco, CA, USA). A typical experiment included untreated control cells for establishing a baseline, and cells treated with 100 μM paraquat (Tokyo Kasei, Tokyo, Japan) as the positive control, which were incubated at 37°C in a humidified atmosphere of 5% CO_2 for 25 minutes to induce ROS production. A gate was set to include only erythrocytes and to exclude reticulocytes, nucleated RBCs (normoblasts), and white blood cells. A 488-nm argon laser beam was used for excitation. The histograms and dot-plotted mean fluorescence intensity were analyzed using Cell Quest software (Beckman Coulter, Inc.) [33,34].

Statistical analyses

Statistical comparisons were performed by the analysis of variance (ANOVA) (ANOVAM: Ver.0.04, Seoul, Korea). To determine the statistical significance of difference, quantitative PCR data were subjected to single-tailed Student's *t*-test. Significant differences between groups were determined by two-way ANOVA ($p < 0.05$). All of the data are presented as the mean ± standard error of the mean.

Results

Effect of benzene toxicity on blood parameters according to Trx genotype

Benzene exposure for 6 hours/day, 5 days/week, for 2 weeks decreased the percentage of white blood cells in peripheral blood and the percent cellularities of femoral BM cells in the Wt controls as indicated by hatched columns in Figure 2A (57.1% and 52.2% for white blood cells; 68.0% and 61.0% for the BM cells, respectively, with respect to the sham-exposed controls expressed as 100%). These results are comparable to those of a previous report [23]. In the h-Trx-Tg mice (solid columns), the decreases were statistically significantly attenuated as compared with those in the Wt groups (each hatched column) (91.2% vs 52.2% for white blood cells, $p < 0.05$, and 87.0% vs 61.0% for BM cells, $p < 0.05$; with respect to each sham-exposed group). Whereas lymphocyte counts in Wt mice decreased specifically after benzene exposure from 50.6 ± 3.0 to 11.8 ± 1.4 × 10^2/μL (i.e., decreased to 23.3% of control), the Tg mice showed no significant decrease in white blood cell (WBC) count, and the decrease in lymphocyte counts was also not significant (43.7 ± 1.9 to 41.9 ± 1.1 × 10^2/μL). In the $Trx^{+/-}$ mice (open columns in this figure), although benzene toxicity in this group was supposed to be exaggerated, the decreases were not significantly different from those in Wt mice (hatched columns) (75.0% vs 57.1% for white blood cells and 61.5% vs 68.0% for BM cells; with respect to each sham-exposed group). Thus, the hemizygous Trx deficiency may not be significantly insufficient for induction of benzene-mediated BM toxicity. Statistically less significant decreases in the percentage of RBCs observed in the Wt, h-Trx-Tg, and $Trx^{+/-}$ mice (hatched, solid, and open columns, respectively) might be due to the early observation of prolonged anemia.

Figure 2B shows the comparison of the percentage of hemopoietic progenitor cells, CFU-GMs, after benzene exposure between the $Trx^{+/-}$ mice and Wt mice (left), and that

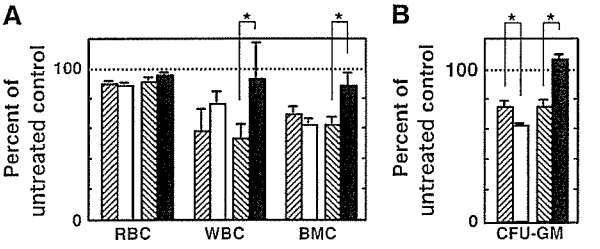

Figure 2. **(A)** Changes in peripheral blood parameters from three mice of each genotype, namely, the percentage numbers of red blood cells (RBCs) and white blood cells (WBCs), and bone marrow cellularity (BMC), after benzene exposure, for 6 h/d, 5d/wk, for 2 weeks. Open columns indicate $Trx^{+/-}$ mice; solid columns, h-Trx-Tg mice; compared with Wt mice, hatched columns. All the columns indicate % of sham-exposed control mice of each genotype. Note that experiments using $Trx^{+/-}$ and h-Trx-Tg mice were conducted separately with Wt mice in each littermate, and are thus indicated by hatched columns in opposite directions. **(B)** Changes in percentage number of CFU-GMs after benzene exposure for 6 h/d, 5 d/wk, for 2 weeks. A mixture of BM cells from three mice of each genotype was used. Open column indicates $Trx^{+/-}$ mice, which show a marked decrease in the percentage number of CFU-GMs as compared with the benzene-exposed Wt mice (hatched column on the far left). The h-Trx-Tg mice (solid column) showed no changes in percentage relative to the sham-exposed h-Trx-Tg mice, whereas the benzene-exposed Wt mice (hatched column, second from the right) showed a significant decrease.

between the h-Trx-Tg mice and Wt mice (right). In contrast to data shown in Figure 2A, the percentage of CFU-GMs in the $Trx^{+/-}$ mice more significantly decreased than that in the Wt mice (hatched columns) (62.4% vs 74.4%, $p < 0.05$; with respect to each sham-exposed group), whereas that in the h-Trx-Tg mice did not decrease at all compared with that in the Wt mice (hatched columns) (100% vs 74.4%, $p < 0.05$; with respect to each sham-exposed group).

CYP2E1 gene expression in BM

The oxidation of benzene metabolites is mediated by CYP2E1, which is a prerequisite for cellular toxicity caused by benzene exposure [35,36]. Whether AhR induction modulates the expression of CYP2E1 remain unclarified [28]. To evaluate any differences in CYP2E1 expression between the Wt and Tg mice exposed to benzene at 300 ppm for 6 hours/day, 5 days/week, for 2 weeks, the expression level of CYP2E1 mRNA was determined by RT-PCR analysis (Fig. 3). There were no significant differences in expression level between the two genotypes. Thus, the induction of hematotoxic benzene metabolites by the increase in CYP2E1 mRNA expression level with time after benzene inhalation started regardless of the genotype, that is, Wt mice or h-Trx-Tg mice. Furthermore, *Trx* overexpression is not expected to play a role in benzene metabolism in relation to CYP2E1 expression in BM.

Expression of transgenic h-Trx and endogenous m-Trx genes

Because the transgene was constructed such that it was constitutively expressed, the expression level of h-*Trx* in the Tg mice was stable during the steady state, as shown in Figure 4A (open squares), and remained stable during and after the benzene inhalation, as shown in Figure 4A (closed squares). During benzene inhalation, m-*Trx* gene expression level, on the other hand, increased transiently, then decreased until day 12, and started to return to the baseline after the cessation of benzene exposure in the Wt mice (Fig. 4B). During benzene exposure, h-Trx-Tg mice showed a temporary increase in the expression level of the endogenous m-*Trx* gene on day 3 post benzene inhalation as compared with the Wt mice on day 1, and then showed a slight decrease by day 12 as compared with the Wt mice, which showed a marked decrease. Thus, changes in endogenous m-*Trx* expression level in the h-Trx-Tg mice were more attenuated than those in the Wt mice during benzene exposure. Moreover, the total Trx activity normalized by GAPDH expression level in the h-Trx-Tg mice during the steady state was nearly twice that in the Wt mice, because both hTrx and mTrx activities on day 0 in the h-Trx-Tg mice were 0.97 and 0.95, respectively.

Induction of SOD activity by benzene inhalation in BM

Because the expression level of endogenous m-*Trx* decreased with benzene exposure duration and it was also shown that the expression of SOD was upregulated by *Trx* in an in vitro study [37], it is of interest to determine SOD activity in the steady state and during benzene exposure. Figure 5 shows SOD activities in the $Trx^{+/-}$ mice (left) and Tg mice (right) with respect to those in the counterpart Wt mice (front columns are for the steady state and back columns are for the benzene exposure). Analogous to the upregulation of SOD activity observed in vitro

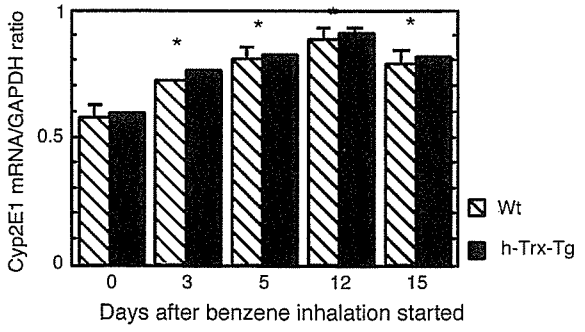

Figure 3. Total RNA was extracted from BM cells from three mice of each genotype at each time point. The expression levels of CYP2E1 mRNA during benzene exposure in the Wt mice and h-Trx-Tg mice were determined by RT-PCR analysis. The ordinate (y-axis) shows the ratio of mRNA expression level of CYP2E1 to that of GAPDH on 0, 3, 5, and 12 days of benzene exposure, and 15 days, that is, 12 days of exposure plus 3 days recovery, in the Wt and h-Trx-Tg mice. Solid columns indicate the expression level in h-Trx-Tg mice, and hatched columns, in the Wt mice. Continuous and statistically significant increases in CYP2E1 mRNA expression level from day 0 to day 12 were observed in both Wt mice and h-Trx-Tg mice, although there were no significant differences in the level between Wt mice and h-Trx-Tg mice. Asterisks indicate statistically significant differences with respect to the steady state, that is, day 0.

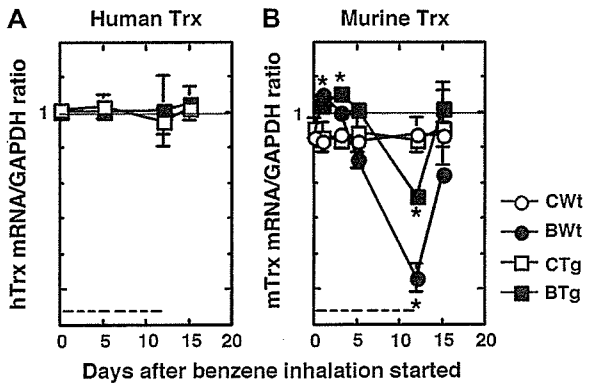

Figure 4. h-*Trx* **(A)** and m-*Trx* **(B)** gene expressions during benzene exposure. Total RNA was extracted from BM cells from three mice of each genotype at each time point. The y-axis indicates the ratio of mRNA expression level of h-*Trx* to that of GAPDH **(A)** and that of m-*Trx* to that of GAPDH **(B)**, vs the days after benzene exposure indicated by a dotted line at the bottom. Benzene-exposed groups (closed squares, h-Trx-Tg mice; BTg: closed circles, Wt mice; BWt) and sham-exposed groups (open squares, h-Trx-Tg mice; CTg: open circles, Wt mice; CWt). Asterisks indicate a significant difference between the benzene-exposed and sham-exposed groups ($p < 0.05$).

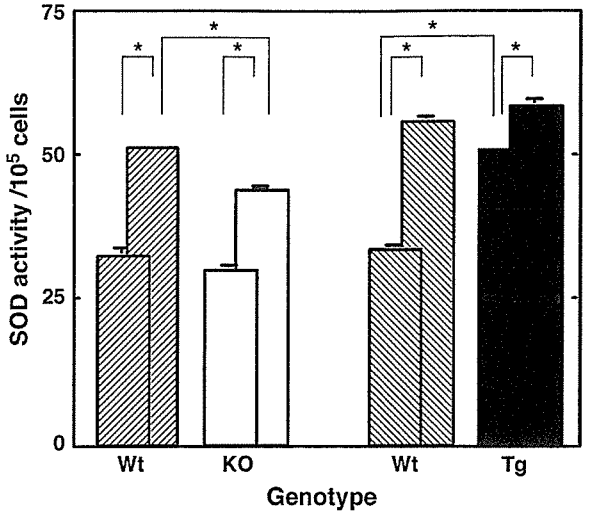

Figure 5. Superoxide dismutase (SOD) activity in BM. During the steady state (left, front columns) and benzene exposure (right, back columns), SOD activities in three mice of each of $Trx^{+/-}$ mice (open columns) and h-Trx-Tg mice (closed column) are compared with those in the Wt mice (hatched columns). A significant upregulation of SOD activity was observed in the h-Trx-Tg mice compared with Wt in the steady state (*: $p < 0.05$), whereas all the benzene-exposed groups showed a significant increase in SOD activity compared with their counterparts in the steady state (*:$p < 0.05$). Furthermore, the relative increase in SOD activity in the Wt mice is significantly larger than that in the $Trx^{+/-}$ mice. Note that the upregulation of SOD activity in the benzene-exposed $Trx^{+/-}$ mice is limited compared with that in the Wt mice. Moreover, the percent upregulations of SOD activity in the steady state and during benzene exposure in the h-Trx-Tg mice are lower than those in the Wt mice (113.3% vs 166.3%).

attributable to the upregulation of Trx [37], we observed this upregulation in the h-Trx-Tg mice at the in vivo level in the steady state as compared with the Wt control (Fig. 5, front columns; Tg, far right, 51.4% vs Wt, second from right, 33.4% inhibition of NTB). During benzene exposure (shown by back columns), SOD activity increased as compared with the steady state, both in the Wt and h-Trx-Tg mice, although the ratio of increase relative to the steady state was larger in the Wt mice than in the h-Trx-Tg mice (Fig. 5, right four columns). Such SOD activity induction by benzene inhalation was observed but to a significantly lesser extent when endogenous *Trx* was deficient (Fig. 5, back columns; KO, second from left, 43.0% vs Wt, far left, 51.0% inhibition of NTB).

Evaluation of ROS amount in tissue during benzene inhalation

Various defense mechanisms against ROS function together, including those involving enzymes such as Trx and SOD; thus, the total amount of ROS accumulated in tissues needs to be evaluated in an in vivo system. We evaluated the intracellular redox status using an oxidation-sensitive dye, DCFH-DA. A significant increase in ROS generation was observed in Wt mice erythrocytes but not in h-Trx-Tg mice erythrocytes, as shown in Figure 6.

Attenuation of cell cycle–related gene expression, p21, by Trx

During benzene exposure, the upregulation of p21, a cyclin-dependent kinase inhibitor, followed by p53 activation suppresses the cell cycle of hemopoietic progenitors, which is known to lead to the repair of damaged DNA [23,38]. However, in mice overexpressing h-*Trx*, the expression levels of both p21 mRNA and its protein did not increase, but rather remained the same. This implies that the repair of DNA damage caused by benzene exposure does not require p21 expression induction in the h-Trx-Tg mice. On the other hand, the expression levels of p21 mRNA and its protein in Wt mice showed a continuous and statistically significant increase with exposure duration as reported previously (Fig. 7) [23]. In the steady state, on the other hand, it is of particular interest that the expression level of p21 mRNA was higher in the h-Trx-Tg mice than in the Wt mice, which may be due to the observed enhancement of *p53* transcription by Trx, resulting in p21 overexpression in the steady state [39].

Decrease in incidence of micronucleated reticulocytes by Trx overexpression

In Figure 8, the incidence of micronucleated reticulocytes (MN-Rets) is shown in percentage along with the duration

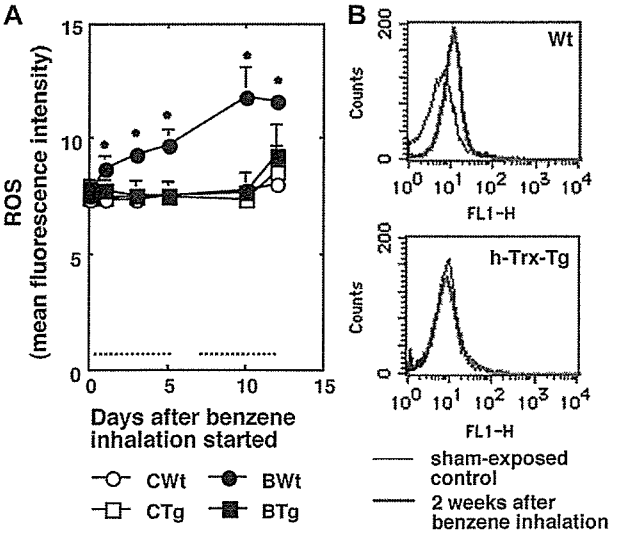

Figure 6. ROS in peripheral RBCs collected from the same three mice of each genotype during benzene inhalation. The total amount of ROS accumulated in RBCs was measured by labeling with DCFH-DA in an in vivo system **(A)** (see Materials and methods). Sample data obtained on day 12, Wt mice on the top and h-Trx-Tg at the bottom **(B)**. With benzene exposure, fluorescence intensity (F.I.) for the BWt mice (closed circles) steadily increased until day 12, whereas F.I. for all other groups remained unchanged. All the data points for the BWt mice showed statistically significant increases as compared with those for the sham-exposed control CWt (*: $p < 0.05$).

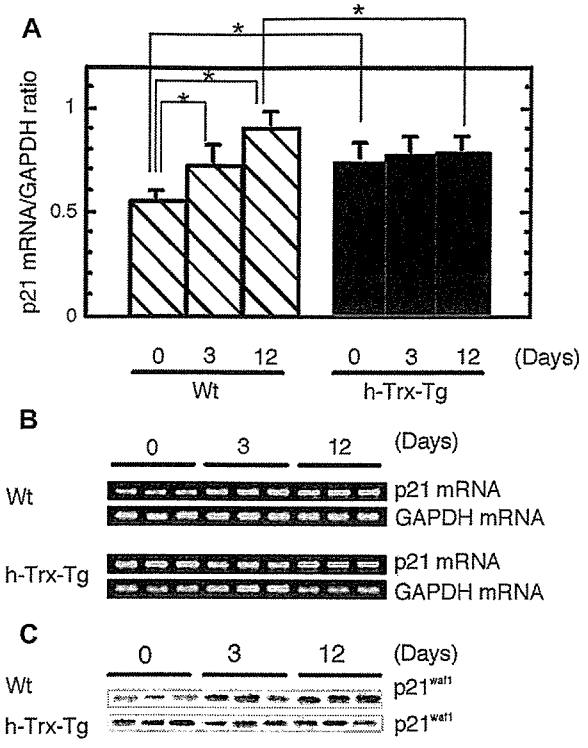

Figure 7. **(A,B)** Expression levels of p21 mRNA in Wt mice and h-Trx-Tg mice during benzene exposure **(B)** and their relative signal intensities **(A)**. The y-axis shows the ratio of mRNA expression level of p21 to that of GAPDH 0, 3, and 12 days after benzene exposure started in the Wt and h-Trx-Tg mice. A continuous and statistically significant increase in p21 mRNA expression level from day 0 to day 12 was observed in the Wt mice ($p < 0.05$), whereas a less significant stable expression was observed in the h-Trx-Tg mice. The level of p21 mRNA expression in h-Trx-Tg mice was higher than that in the Wt mice at the steady state, which may be explained by the observation that *Trx* enhanced the transcription of p53, resulting in this overexpression at the steady state **(A,B)**. Furthermore, the attenuation of DNA damage caused by benzene exposure did not seem to induce p21 expression in the h-Trx-Tg mice, although p21 mRNA expression level in Wt mice continuously and statistically significantly increased with exposure duration as reported previously (*: $p < 0.05$). **(C)** Comparable protein expression levels are observed at the steady state and during benzene exposure.

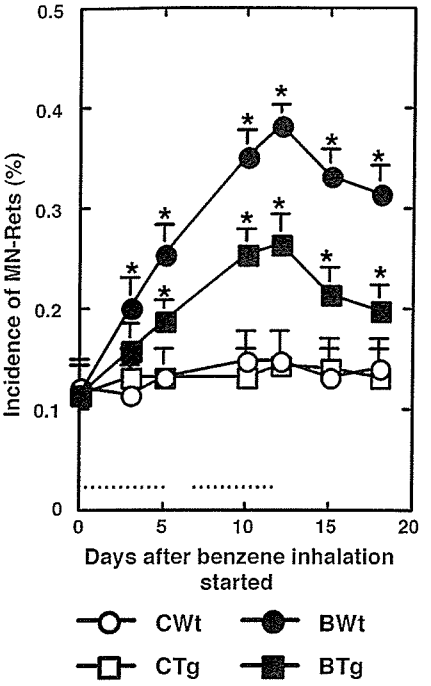

Figure 8. Time course of sequential changes in incidence of MN-Rets. Closed symbols indicate mice exposed to benzene at 300 ppm for 6 h/d, 5 d/wk, for 2 weeks as indicated by a dotted line at the bottom of the graph. After day 12, all the mice were removed from the inhalation chambers until day 18 and compared with sham-exposed groups (open symbols). Circles and squares indicate Wt groups and h-Trx-Tg groups, respectively. Both the benzene-exposed groups, BWt and BTg, showed significantly higher incidences of MN-Rets than the sham-exposed groups, CWt and CTg, 3, 5, 10, 12, 15, and 18 days after starting benzene exposure (asterisks on the closed circle, BWt : $p < 0.05$). The BWt mice (top, closed circles) showed a higher incidence (%) of MN-Rets, whereas the BTg mice (second from top, closed squares) showed about 48% decrease throughout the observation period. A significantly lower MN-Ret incidence in benzene-exposed BTg than in BWt on days 5, 10, 12, 15, and 18 (asterisks on the closed squares, BTg: $p < 0.05$) was observed.

of benzene exposure. The mice were exposed to benzene at a dose of 300 ppm for 6hours/day, 5 days/week, for 2 weeks as shown in the exposure schedule indicated by a dotted line at the bottom of Figure 8. On day 12, all the mice were removed from the inhalation chamber and maintained without benzene inhalation until day 18. The incidence of MN-Rets in the Wt group, indicated by closed circles (top), increased with the number of days of exposure to benzene until day 12. It then started to return to the baseline after the termination of benzene exposure. Interestingly, the h-Trx-Tg mice (closed squares) showed a lower incidence of about 52% than the Wt group on day 12, as shown by a lower peak (0.12% and 0.23% increases in sham-exposed h-Trx-Tg and Wt mice, respectively), which then started to decrease after the termination of benzene exposure. Open squares and circles represent sham-exposed Wt and h-Trx-Tg groups, respectively.

Lifetime incidence of lympho-hematopoietic malignancies

To investigate a possible inhibition of the development of benzene-induced lympho-hematopoietic neoplasms after benzene inhalation, a lifetime bioassay of h-Trx-Tg mice exposed to intermittent benzene inhalation at 300 ppm for 26 weeks was conducted in comparison with Wt mice. The survival curves are shown in Figure 9A. The curve of sham-exposed h-Trx-Tg mice shows a survival of 1111.5 days; that is, 298 days longer than the median lifetime as compared with that in Wt mice (thinner dotted line vs thinner solid line, respectively). In the groups exposed to benzene, when the survival curve of h-Trx-Tg mice (bold dotted line) is compared with that of the Wt mice, the former again shows a longer survival curve, although in the

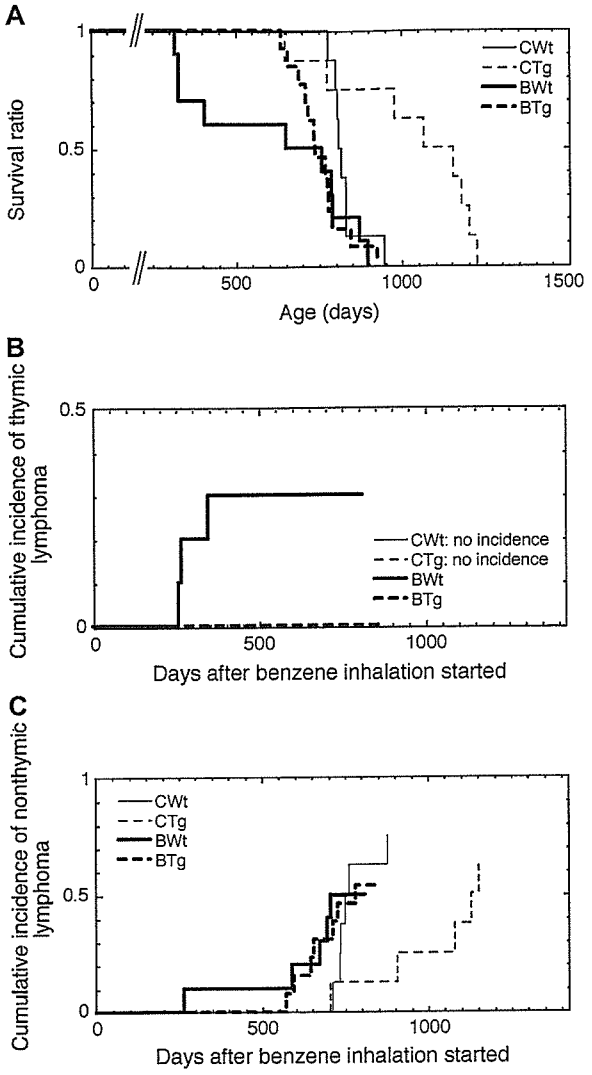

Figure 9. For lymphomagenicity studies, the numbers of mice per group, namely, Wt mice with (designated as B in the figure) or without (designated as C in the figure) benzene exposure, and Tg mice with or without benzene exposure, were 10 BWt mice, 8 CWt mice, 13 BTg mice, and 8 CTg mice. Survival curve (**A**) and incidences of thymic lymphoma (**B**) and nonthymic lymphoma (**C**) are shown. Thin solid line, sham-exposed Wt group (CWt); bold solid line, benzene-exposed Wt group (BWt); thin dotted line, sham-exposed Trx group (CTg); and bold dotted line, benzene-exposed Trx group (BTg). No thymic lymphomas were observed in the CWt, CTg, and BTg groups.

later part, after 750 days of age, the survival curves of the h-Trx-Tg mice and Wt mice are not significantly different from each other. As shown in Figure 9B and C, benzene exposure at 300 ppm for 26 weeks induced hemopoietic malignancies, namely, thymic lymphomas (Fig. 9B) and nonthymic lymphomas (Fig. 9C). Whereas the cumulative incidence of thymic lymphomas reached the maximum of 30% in the Wt mice by day 350, surprisingly, no thymic lymphomas developed in the h-Trx-Tg group (Fig. 9B). Figure 9C, on the other hand, shows comparable cumulative incidences of benzene-induced nonthymic lymphomas (bold dotted line vs bold solid line, respectively), between the h-Trx-Tg mice (53.8%) and the Wt mice (50.0%), whereas the sham-exposed groups of h-Trx-Tg mice and Wt mice show slightly higher incidences than the benzene-exposed groups (62.5% and 75.0%, respectively) with identical onsets but a much larger time lag (thinner dotted line vs thinner solid line, respectively).

AhR mRNA expression in BM

Our previous study showed that benzene toxicity is transmitted by AhR [28]. It is of interest to examine *AhR* gene expression in the h-Trx-Tg mice after benzene inhalation. The expression level of AhR mRNA significantly decreased to one-half of the steady-state level on days 5 and 12 of benzene inhalation only in the h-Trx-Tg mice (Fig. 10A, right, and B, bottom), whereas there were no significant differences in AhR mRNA expression level at the steady state between the Wt mice and h-Trx-Tg mice (Fig. 10A, Wt and h-Trx-Tg on day 0). Furthermore, the expression level of AhR mRNA in the Wt mice did not change throughout the exposure period (Fig. 10A, left, and B, top).

Discussion

The thioredoxin gene–modified mice, $Trx^{+/-}$ mice and h-Trx-Tg mice, responded to ROS in a *Trx* gene–dose-dependent manner not only in mature BM cells but also in progenitor cells, CFU-GMs (Fig. 2B). The exacerbation

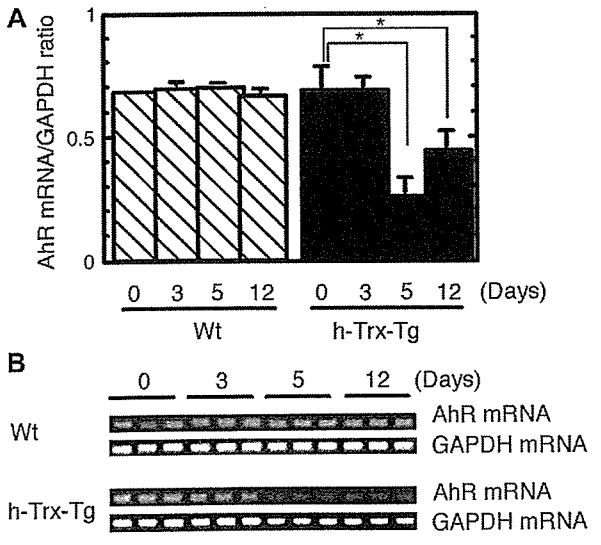

Figure 10. (**A,B**) Expression levels of AhR mRNA in Wt mice and h-Trx-Tg mice during benzene exposure (**A**), and their relative signal intensities (**B**). The y-axis shows the ratio of mRNA expression level of AhR to that of GAPDH 0, 3, 5, and 12 days after benzene exposure started in the Wt and h-Trx-Tg mice. The expression of AhR mRNA in the h-Trx-Tg mice was downregulated after benzene exposure started, and the expression levels on days 5 and 12 significantly decreased to 35.9% and 63.4% of those in the steady state, respectively (*: $p < 0.05$).

of benzene-induced hemato-lymphoid toxicity in the $Trx^{+/-}$ mice in combination with the attenuation of that in the h-Trx-Tg mice has confirmed for the first time at the whole-animal level that the hemato-lymphoid toxicity of benzene is caused by oxidative stress from ROS (Fig. 2B). These correlations were not observed for RBCs (Fig. 2A), because of the very short period (2 weeks) of benzene exposure for RBC turnover to induce anemia in peripheral blood. For WBCs and BM cellularity (BMC), significant correlations were not observed either, but because of heteroinsufficiency (see Materials and methods; homozygosity is fatal) in giving rise to a knockout phenotype, although attenuation in hemizygous overexpression (h-Trx-Tg) was significant for both blood parameters.

Whether the different benzene toxicities observed in h-Trx-Tg and Wt mice may have been caused by a difference in ROS generation or a difference in repair potential between h-Trx-Tg and Wt mice, may be clarified by examining the expression level of CYP2E1 in the h-Trx-Tg and Wt mice. The identical CYP2E1 expression levels not only in the Wt mice but also in h-Trx-Tg mice suggest a possible induction of ROS even in h-Trx-Tg mice (Fig. 3).

However, interestingly, ROS level evaluated using DCFH-DA did not increase at all in the h-Trx-Tg mice as shown in Figure 6 (BTg, closed squares; benzene-exposed Tg mice). *How were generated ROS removed in the h-Trx-Tg mice?* The major factor for ROS scavenging in the h-Trx-Tg mice appears to be transgenic h-Trx, which is constitutively expressed throughout the benzene exposure period as shown in Figure 4A. In the h-Trx-Tg mice, SOD activity was upregulated owing to the constitutive expression of h-Trx even without benzene exposure, and in the case of benzene exposure, SOD activity was further upregulated to the same level as that in the Wt mice (Fig. 5, Tg, dark pair columns on the far right compared with Wt, shaded pair columns on the second from far right). The reasons for the limited upregulation of SOD activity in the h-Trx-Tg mice with benzene exposure may be as follows. First, SOD activity was evaluated on day 12, i.e., corresponding to the lowest level of m-Trx-mRNA expression (Fig. 4B). Second, there could be a sufficient scavenging capacity in h-Trx-Tg mice when ROS level was evaluated using DCFH-DA (Fig. 6). A higher SOD activity was observed during the steady state of h-Trx-Tg than the Wt mice, because the total Trx activity normalized by GAPDH expression level in the h-Trx-Tg mice during the steady state was nearly twice (hTrx + mTrx) that in the Wt mice (0.96 + 1.01 vs 0.93, respectively). This may agree with the extent of upregulation of SOD activity in the h-Trx-Tg mice during the steady state (51.4%).

On the other hand, ROS production continued during benzene exposure in the Wt mice (Fig. 6). During this period, de novo m-Trx was induced initially on day 1 and then its level decreased even during the second week of benzene exposure, followed by a rapid return to the baseline after the termination of exposure (Fig. 4B, closed circles). This trend of m-Trx production in the Wt mice was attributable to the increase in SOD activity in the steady state compared with SOD activity during benzene exposure of mice despite the rapid downmodulation of Trx from the steady-state level. Because SOD activity is induced by Trx, the induction of SOD in the $Trx^{+/-}$ mice is enhanced significantly by benzene exposure but to a lesser extent than that in the steady state, which is significantly lower than that in the benzene-exposed Wt mice (Fig. 5, open back column vs corresponding shaded back column). (Note that the $Trx^{+/-}$ mice showed an expression level 50% of that of m-Trx owing to hemizygosity; see Fig. 1). When one examines the ROS level of benzene-exposed Wt mice (Fig. 6, closed circles), it increases with time after benzene inhalation, indicating that the above-mentioned de novo Trx and SOD inductions were not effective in removing such ROS. Despite the complete elimination of ROS in h-Trx-Tg mice, it is interesting that milder and delayed responses were observed in m-Trx expression in the h-Trx-Tg mice during benzene inhalation (Fig. 4B, closed squares), implying that local ROS may not be readily eliminated, but there may be some time lag.

The scavenging of ROS in h-Trx-Tg mice was supposed not to show any increase in the expression level of p21-mRNA throughout the benzene exposure period, although the level was rather higher than that in the Wt mice in the steady state. This may be due, in part, to the upregulation of the transcriptional activity of p53 known to be induced by Trx [39], contributing to a possible efficient repair of steady-state DNA damage by a decelerated cell cycle during benzene exposure (Fig. 7). In the Wt mice, p21 level was upregulated with benzene exposure duration as compared with the level of that in the steady state. This is consistent with a previous study revealing the expression of p21 in the Wt mice followed by the upregulation of p53, which is, vice versa, nullified in the p53 KO mice [23]. The expression level of p21 on day 12 in the Wt mice was higher than that in the h-Trx-Tg mice, implying that DNA damage caused by accumulated ROS is milder in the h-Trx-Tg mice.

In the present study, it was surprising that the incidence of thymic lymphoma was 0% in the h-Trx-Tg mice (Fig. 9B). Nonthymic lymphoma development, on the other hand, was not attenuated (Fig. 9C), which does not necessarily suggest that the lymphomagenesis of nonthymic lymphomas is due to ROS. The nontreated control mice are genetically predisposed to developing nonthymic lymphomas as they age. Regardless of the genotype, that is, Wt or Trx-Tg mice, this process may be accelerated in benzene-treated animals in an h-Trx-independent manner; but this plausibility cannot be confirmed in the present study. Also, whether significant lymphoid cell depletion after benzene exposure and its attenuation in Trx-Tg mice has any possible relevance to the incidence of lymphomagenesis

and its attenuation in Trx-Tg mice cannot be clarified in the present study.

Because thymic lymphoma generally does not develop spontaneously in our breeding colony of C57BL/6 mice, and benzene exposure preferentially induces thymic lymphoma rather than nonthymic lymphoma [40], these imply that h-Trx overexpression in the present study likely attenuates solely the benzene-induced increase in the incidence of hemopoietic malignancies [41]. Along with the decrease in the incidence of MN-Rets in the h-Trx-Tg mice (Fig. 8), the prevention of benzene-induced thymic and nonthymic lymphomagenicities in the Tg mice as shown in Figure 9B also confirmed that thymic lymphoma was induced by oxidative stress.

The last unresolved question is why the incidence of nonthymic lymphoma did not decrease in the h-Trx-Tg mice, which seemed to be related to the insufficient decrease in MN-Ret incidence in the h-Trx-Tg mice. There seems to be an inconsistency between this insufficient decrease in MN-Ret incidence and the almost complete clearance of ROS as shown in Figure 6. An interpretation of this inconsistency remains hypothetical, but thymic lymphoma cells may preferentially develop under leukocyte chemotaxis and chemokine exposure, which may be specifically induced by benzene-induced oxidative stress. When Trx is overexpressed, such leukocyte chemotaxis as well as chemokine expression may be suppressed and thymic lymphoma may not develop under such circumstances anymore [42]. In another aspect, Trx overexpression may preferentially enhance p53-dependent apoptosis even when thymic lymphoma developed. These possibilities may be relevant to the observations that thymic lymphoma seems to be a neoplasm only induced by benzene exposure, and nonthymic lymphoma is considered to develop spontaneously [43,44]. Consistently, the incidence of MN-Rets increased in the Wt mice during benzene exposure, which then decreased after the cessation of exposure, whereas in the h-Trx-Tg mice, on the other hand, the incidence of MN-Rets markedly decreased (Fig. 8). Also, a possible explanation is due to immunosuppression induced by benzene-related pro-hapten, and its consequent increase in stress level, which may lead to ROS-independent lymphomagenicity.

It is of interest to examine AhR gene expression. Because our previous study showed that benzene-induced hemato-lymphoid toxicity is transmitted via AhR and that AhR-KO mice surprisingly do not show any benzene-induced hemato-lymphoid toxicity [28], the significant downregulation of AhR observed solely in the h-Trx-Tg mice may be another factor contributing to the attenuation of benzene-induced hemato-lymphoid toxicity in the h-Trx-Tg mice. This downmodulation of AhR, specifically observed in the h-Trx-Tg mice, did not make any difference in the expression level of CYP2E1 in the present study; therefore, the mechanistic background underlying the difference in ROS production between Wt mice and h-Trx-Tg mice in relation to this downmodulation is yet to be determined.

Acknowledgments

This work was supported in part by the Human Sciences of Japan (KH31034), Grant-in-Aid for Scientific Research C (Nos. 15510064 and 16590329), the fund from Nuclear Research of the MEXT, Japan, and also the MHLW-Research Fund (H16-Chemistry0002) National Institute of Health Sciences.

We thank Ms. E. Tachihara, Ms. Y. Usami, Ms. Y. Shinzawa, Ms. M. Uchiyama, Mr. K. Terasaka, and Ms. C. Aoyagi for excellent technical assistance. We also thank Drs. M. Hayashi, H. Masutani, and K. Igarashi for valuable advice, and Ms. Y. Kikuchi, Ms. N. Katsu, Ms. M. Yoshizawa, and Ms. M. Hojo for secretarial assistance.

References

1. Golding BT, Watson WP. Possible mechanisms of carcinogenesis after exposure to benzene. IARC Sci Publ. 1999;75–88.
2. Madl AK, Paustenbach DJ. Airborne concentrations of benzene due to diesel locomotive exhaust in a roundhouse. J Toxicol Environ Health A. 2002;65:1945–1964.
3. Mitacek EJ, Brunnemann KD, Polednak AP, Limsila T, Bhothisuwan K, Hummel CF. Rising leukemia rates in Thailand: the possible role of benzene and related compounds in cigarette smoke. Oncol Rep. 2002; 9:1399–1403.
4. Aksoy M, Erdem S, DinCol G. Leukemia in shoe-workers exposed chronically to benzene. Blood. 1974;44:837–841.
5. Yin SN, Hayes RB, Linet MS, et al. An expanded cohort study of cancer among benzene-exposed workers in China. Benzene Study Group. Environ Health Perspect. 1996;104:1339–1341.
6. Lan Q, Zhang L, Li G, et al. Hematotoxicity in workers exposed to low levels of benzene. Science. 2004;306:1774–1776.
7. Ross D. The role of metabolism and specific metabolites in benzene-induced toxicity: evidence and issues. J Toxicol Environ Health A. 2000;61:357–372.
8. Lewis JG, Stewart W, Adams DO. Role of oxygen radicals in induction of DNA damage by metabolites of benzene. Cancer Res. 1988; 48:4762–4765.
9. Parke DV. Personal reflections on 50 years of study of benzene toxicology. Environ Health Perspect. 1996;104(Suppl 6):1123–1128.
10. Dean BJ. Genetic toxicology of benzene, toluene, xylenes and phenols. Mutat Res. 1978;47:75–97.
11. Dean BJ. Recent findings on the genetic toxicology of benzene, toluene, xylenes and phenols. Mutat Res. 1985;154:153–181.
12. Creek MR, Mani C, Vogel JS, Turteltaub KW. Tissue distribution and macromolecular binding of extremely low doses of [14C]-benzene in B6C3F1 mice. Carcinogenesis. 1997;18:2421–2427.
13. Mazzullo M, Bartoli S, Bonora B, et al. Benzene adducts with rat nucleic acids and proteins: dose-response relationship after treatment in vivo. Environ Health Perspect. 1989;82:259–266.
14. Lutz WK. Quantitative evaluation of DNA binding data for risk estimation and for classification of direct and indirect carcinogens. J Cancer Res Clin Oncol. 1986;112:85–91.
15. Snyder R, Hedli CC. An overview of benzene metabolism. Environ Health Perspect. 1996;104(Suppl 6):1165–1171.
16. Siou G, Conan L, el Haitem M. Evaluation of the clastogenic action of benzene by oral administration with 2 cytogenetic techniques in mouse and Chinese hamster. Mutat Res. 1981;90:273–278.

17. Winn LM. Homologous recombination initiated by benzene metabolites: a potential role of oxidative stress. Toxicol Sci. 2003;72:143–149.
18. Takagi Y, Mitsui A, Nishiyama A, et al. Overexpression of thioredoxin in transgenic mice attenuates focal ischemic brain damage. Proc Natl Acad Sci U S A. 1999;96:4131–4136.
19. Mitsui A, Hirakawa T, Yodoi J. Reactive oxygen-reducing and protein-refolding activities of adult T cell leukemia–derived factor/human thioredoxin. Biochem Biophys Res Commun. 1992;186:1220–1226.
20. Hirabayashi Y. p53-dependent gene profiling for reactive oxygen species after benzene inhalation: special reference to genes associated with cell cycle regulation. Chem Biol Interact. 2005;153–154:165–170.
21. Matsui M, Oshima M, Oshima H, et al. Early embryonic lethality caused by targeted disruption of the mouse thioredoxin gene. Dev Biol. 1996;178:179–185.
22. Cronkite EP, Bullis J, Inoue T, Drew RT. Benzene inhalation produces leukemia in mice. Toxicol Appl Pharmacol. 1984;75:358–361.
23. Yoon BI, Hirabayashi Y, Kawasaki Y, et al. Mechanism of action of benzene toxicity: cell cycle suppression in hemopoietic progenitor cells (CFU-GM). Exp Hematol. 2001;29:278–285.
24. Hirabayashi Y, Matsuda M, Aizawa S, Kodama Y, Kanno J, Inoue T. Serial transplantation of p53-deficient hemopoietic progenitor cells to assess their infinite growth potential. Exp Biol Med (Maywood). 2002; 227:474–479.
25. Hayashi M, Morita T, Kodama Y, Sofuni T, Ishidate M Jr. The micronucleus assay with mouse peripheral blood reticulocytes using acridine orange–coated slides. Mutat Res. 1990;245:245–249.
26. Frith CH, Ward JM, Harleman JH, et al. Hematopoietic system. In: Mohr U, ed. International Classification of Rodent Tumor: The Mouse. Heidelberg: Springer; 2001. p. 417–451.
27. Hirabayashi Y, Inoue T, Suda Y, Aizawa S, Ikawa Y, Kanisawa M. Hemopoietic neoplasms in lethally irradiated mice repopulated with bone marrow cells carrying the human c-myc oncogene: a repopulation assay. Exp Hematol. 1992;20:167–172.
28. Yoon BI, Hirabayashi Y, Kawasaki Y, et al. Aryl hydrocarbon receptor mediates benzene-induced hematotoxicity. Toxicol Sci. 2002;70: 150–156.
29. Fridovich I. Quantitative aspects of the production of superoxide anion radical by milk xanthine oxidase. J Biol Chem. 1970;245:4053–4057.
30. Bass DA, Parce JW, Dechatelet LR, Szejda P, Seeds MC, Thomas M. Flow cytometric studies of oxidative product formation by neutrophils: a graded response to membrane stimulation. J Immunol. 1983;130: 1910–1917.
31. Royall JA, Ischiropoulos H. Evaluation of 2′, 7′-dichlorofluorescein and dihydrorhodamine 123 as fluorescent probes for intracellular H_2O_2 in cultured endothelial cells. Arch Biochem Biophys. 1993; 302:348–355.
32. Frank J, Biesalski HK, Dominici S, Pompella A. The visualization of oxidant stress in tissues and isolated cells. Histol Histopathol. 2000; 15:173–184.
33. Imrich A, Kobzik L. Flow cytometric analysis of macrophage oxidative metabolism using DCFH. Methods Mol Biol. 1998;91:97–108.
34. Amer J, Goldfarb A, Fibach E. Flow cytometric measurement of reactive oxygen species production by normal and thalassaemic red blood cells. Eur J Haematol. 2003;70:84–90.
35. Smith MT. The mechanism of benzene-induced leukemia: a hypothesis and speculations on the causes of leukemia. Environ Health Perspect. 1996;104:1219–1225.
36. Bauer AK, Faiola B, Abernethy DJ, et al. Genetic susceptibility to benzene-induced toxicity: role of NADPH: quinone oxidoreductase-1. Cancer Res. 2003;63:929–935.
37. Das KC, Lewis-Molock Y, White CW. Elevation of manganese superoxide dismutase gene expression by thioredoxin. Am J Respir Cell Mol Biol. 1997;17:713–726.
38. Yoon BI, Li GX, Kitada K, et al. Mechanisms of benzene-induced hematotoxicity and leukemogenicity: cDNA microarray analyses using mouse bone marrow tissue. Environ Health Perspect. 2003;111: 1411–1420.
39. Ueno M, Masutani H, Arai RJ, et al. Thioredoxin-dependent redox regulation of p53-mediated p21 activation. J Biol Chem. 1999;274: 35809.
40. Kawasaki Y, Hirabayashi Y, Yoon BI, et al. Benzene inhalation induced an early onset and a high incidence of leukemias in the p53-deficient C57BL/6 mice. Jpn J Cancer Res. 2001;92:71.
41. Husbeck B, Powis G. The redox protein thioredoxin-1 regulates the constitutive and inducible expression of the estrogen metabolizing cytochromes P450 1B1 and 1A1 in MCF-7 human breast cancer cells. Carcinogenesis. 2002;23:1625–1630.
42. Burke-Gaffney A, Callister ME, Nakamura H. Thioredoxin: friend or foe in human disease? Trends Pharmacol Sci. 2005;26:398–404.
43. Ravi D, Muniyappa H, Das KC. Endogenous thioredoxin is required for redox cycling of anthracyclines and p53-dependent apoptosis in cancer cells. J Biol Chem. 2005;280:40084–40096.
44. Zhou Y, Kok KH, Chun AC, et al. Mouse peroxiredoxin V is a thioredoxin peroxidase that inhibits p53-induced apoptosis. Biochem Biophys Res Commun. 2000;268:921–927.

Meeting Report: Validation of Toxicogenomics-Based Test Systems: ECVAM–ICCVAM/NICEATM Considerations for Regulatory Use

Raffaella Corvi,[1] Hans-Jürgen Ahr,[2] Silvio Albertini,[3] David H. Blakey,[4] Libero Clerici,[5] Sandra Coecke,[1] George R. Douglas,[4] Laura Gribaldo,[1] John P. Groten,[6] Bernd Haase,[7] Karen Hamernik,[8] Thomas Hartung,[1] Tohru Inoue,[9] Ian Indans,[10] Daniela Maurici,[1] George Orphanides,[11] Diana Rembges,[5] Susanna-Assunta Sansone,[12] Jason R. Snape,[13] Eisaku Toda,[14] Weida Tong,[15] Joost H. van Delft,[16] Brenda Weis,[17] and Leonard M. Schechtman[18,19]

[1]European Centre for the Validation of Alternative Methods (ECVAM), Institute for Health and Consumer Protection (IHCP), Joint Research Centre of the European Commission (JRC), Ispra, Italy; [2]Bayer HealthCare AG, Wuppertal, Germany; [3]Hoffmann-La Roche, Basel, Switzerland; [4]Environmental Health Centre, Health Canada, Ottawa, Ontario, Canada; [5]Physico-Chemical Exposure, IHCP, JRC, Ispra, Italy; [6]TNO, Utrecht, the Netherlands; [7]QIAGEN, Hilden, Germany; [8]U.S. Environmental Protection Agency, Washington, DC, USA; [9]National Institute of Health Sciences, Tokyo, Japan; [10]Health Safety Executive, London, United Kingdom; [11]Syngenta, Macclesfield, United Kingdom; [12]European Molecular Biology Laboratory, European Bioinformatics Institute, Hinxton, Cambridge, United Kingdom; [13]AstraZeneca, Brixham, United Kingdom; [14]Organisation for Economic Co-operation and Development, Paris, France; [15]Food and Drug Administration, National Center for Toxicological Research, Jefferson, Arkansas, USA; [16]University of Maastricht, Maastricht, the Netherlands; [17]National Institute of Environmental Health Sciences, National Institutes of Health, Department of Health and Human Services, Research Triangle Park, North Carolina, USA; [18]U.S. Interagency Coordinating Committee on the Validation of Alternative Methods, Research Triangle Park, NC, USA; [19]U.S. Food and Drug Administration, National Center for Toxicological Research, Rockville, Maryland, USA

This is the report of the first workshop "Validation of Toxicogenomics-Based Test Systems" held 11–12 December 2003 in Ispra, Italy. The workshop was hosted by the European Centre for the Validation of Alternative Methods (ECVAM) and organized jointly by ECVAM, the U.S. Interagency Coordinating Committee on the Validation of Alternative Methods (ICCVAM), and the National Toxicology Program (NTP) Interagency Center for the Evaluation of Alternative Toxicological Methods (NICEATM). The primary aim of the workshop was for participants to discuss and define principles applicable to the validation of toxicogenomics platforms as well as validation of specific toxicologic test methods that incorporate toxicogenomics technologies. The workshop was viewed as an opportunity for initiating a dialogue between technologic experts, regulators, and the principal validation bodies and for identifying those factors to which the validation process would be applicable. It was felt that to do so now, as the technology is evolving and associated challenges are identified, would be a basis for the future validation of the technology when it reaches the appropriate stage. Because of the complexity of the issue, different aspects of the validation of toxicogenomics-based test methods were covered. The three focus areas include *a)* biologic validation of toxicogenomics-based test methods for regulatory decision making, *b)* technical and bioinformatics aspects related to validation, and *c)* validation issues as they relate to regulatory acceptance and use of toxicogenomics-based test methods. In this report we summarize the discussions and describe in detail the recommendations for future direction and priorities. *Key words:* acceptance, alternatives, biomarker, predictive test, regulatory use, standardization, toxicogenomics, toxicology, validation. *Environ Health Perspect* 114:420–429 (2006). doi:10.1289/ehp.8247 available via *http://dx.doi.org/* [Online 17 August 2005]

Toxicogenomics, an emerging field in molecular toxicology, offers the promise of new approaches to identify and characterize such factors as the biologic activity of new and existing chemicals and drugs and could play an important role in hazard assessment for human health. This revolutionary field can potentially affect many scientific and medical areas, including the development of a new generation of alternative predictive testing and screening methods that could lend themselves to the reduction, refinement, and replacement of animals used for such purposes.

The European Centre for the Validation of Alternative Methods (ECVAM), the U.S. Interagency Coordinating Committee on the Validation of Alternative Methods (ICCVAM), and the National Toxicology Program Interagency Center for the Evaluation of Alternative Toxicological Methods (NICEATM) are currently investigating the specific considerations necessary for adequate validation of toxicogenomics-based test methods. The primary objective of ECVAM and ICCVAM/NICEATM is to facilitate development, validation, and regulatory acceptance of new, revised, and alternative test methods that reduce, refine, and replace the use of animals (referred to as the three Rs; Russell and Burch 1959) in testing while maintaining and promoting scientific quality and the protection of human health, animal health, and the environment. The efforts of such organizations as ICCVAM/NICEATM and ECVAM have helped foster the principles of the three R's and have contributed to progress in the use of alternative methods for regulatory, research, and educational purposes.

Experience in the validation of conventional alternative test methods has led to an understanding that new and innovative approaches likely will be necessary to standardize test methods based on toxicogenomics and to evaluate the scientific validity and regulatory applicability of such test methods. It is envisioned that the entire validation process will be more complex and challenging than that typically encountered thus far for other alternative test methods. This is because not only will the technology itself need to be standardized and validated, but the methods that are based upon the technology and their predictive aspects will also need to undergo validation if they are to be employed in regulatory decision-making processes. In addition the validation process must be able to accommodate the anticipated rapid changes in technology that could affect the performance of the test method and its reliability for a specific purpose.

Toxicogenomics-based methods are being widely applied in toxicology and biomedical research. Because data are already being generated using these technologies, it is both timely and important to address the subject of validation now with the aim of establishing a foundation that will facilitate future regulatory acceptance of scientifically validated

Address correspondence to R. Corvi, European Centre for the Validation of Alternative Methods, IHCP, Joint Research Centre of the European Commission, Via E. Fermi 1, 21120 Ispra, Italy. Telephone: 39-0332-785266. Fax: 39-0332-785845. E-mail: raffaella.corvi@jrc.it

Supplemental Material is available online (http://ehp.niehs.nih.gov/members/2005/8247/suppl.pdf).

We gratefully acknowledge W.S. Stokes, Director of the National Toxicology Program Interagency Center for the Evaluation of Alternative Toxicological Methods, for contributions to the planning and organization of the workshop as well as insightful and constructive comments.

This document represents the consensus of the participants' views expressed as individual scientists and does not necessarily represent the policies and procedures of their respective institutions.

The authors declare they have no competing financial interests.

Received 22 April 2005; accepted 17 August 2005.

toxicogenomics-based test methods. By addressing the critical validation issues early, and in parallel with the evolutionary and maturation phases of the technologic development of toxicogenomics-based methods, it should be possible to preempt many potential pitfalls and data gaps encountered with retrospective method evaluations that could impede validation of this promising research and regulatory tool. Such a strategy will also facilitate early buy-in and confidence in the technologies by the regulatory arena in its quest for new, improved, and relevant methods by which to help ensure human health, protect the environment, and demonstrate responsiveness to animal welfare issues.

In consideration of all these related issues, ECVAM and ICCVAM/NICEATM held the first of a planned series of workshops to address the validation principles that lend themselves to toxicogenomics-based test methods, for example, gene expression technologies and associated bioinformatics. Given the complexity of the rapidly evolving toxicogenomics field, a variety of issues were addressed. These included but were not limited to *a*) differences in and evolution of technology platforms including changes in genome coverage for model species; *b*) quality assurance (QA) and Good Laboratory Practice (GLP) compliance; *c*) technology standardization, transferability, and reproducibility; *d*) relevance to *in vivo* biological responses; *e*) yardsticks against which toxicogenomics responses should be measured; *f*) data evaluation, statistical approaches, and databases; *g*) validation approaches; and *h*) regulatory acceptability.

To begin to examine these complex issues, three breakout groups were formed. Each group concentrated on different aspects of the validation of toxicogenomics-based test methods, and the discussions were shared with the other participants in plenary sessions. The three focus areas were *a*) biological validation of toxicogenomics-based test methods for regulatory decision making, *b*) technical and bioinformatics aspects related to validation, and *c*) validation issues as they relate to regulatory acceptance and use of toxicogenomics-based test methods.

Validation of Toxicogenomics: Focus on the Biological Systems

The biological issues related to the validation of toxicogenomics-based test methods involved two strategies proposed for developing and validating such methods so that they can be employed to support regulatory decision making. One strategy involves phenotypic anchoring of gene expression changes to identify molecular mechanisms and candidate biomarkers of toxicity (i.e., single genes, proteins, or biological pathways). A second strategy involves the identification and validation of predictive gene expression signatures of toxicity. Validation considerations specific to data quality and cross-platform and interlaboratory variability that are common to both strategies were identified. It is acknowledged that any new toxicogenomics-based methods will need to address established validation criteria for determination of reliability and relevance (Balls et al. 1995; ICCVAM 1997, 2003) as well as articulate the advantages and limitations of a given toxicogenomics-based test method. In addition biological validation of such a test method, that is, assessment of the concordance of gene changes with biological events, is essential but is contingent upon validation of the technology itself, which is addressed elsewhere in this article.

Strategy 1: use of toxicogenomics data to define mechanism and identify biomarkers. Toxicogenomics offers the opportunity to enhance existing toxicity prediction strategies through elucidation of biological mechanisms around critical events. This sentiment is captured in the recent U.S. Environment Protection Agency (EPA) and U.S. Food and Drug Administration (FDA) strategies regarding the inclusion of genomics data in submissions of regulated substances (U.S. EPA 2002; U.S. FDA 2005). Although these agencies currently preclude basing regulatory decision making on genomics data alone, they do encourage the voluntary submission of well-documented, quality genomics data. Both agencies are considering the use of submitted data on a case-by-case basis for assessment purposes (e.g., to help elucidate mechanism of action or contribute to a weight-of-evidence approach) or for populating relevant comparative databases by encouraging parallel submissions of genomics data and traditional toxicologic test results. This approach is appropriate given the state of scientific knowledge of toxicogenomics and the requisite need for a clear understanding of the toxicologic relevance of the gene expression signals detected by this technology. There is a small but rapidly increasing number of published reports demonstrating a linkage between gene expression changes and adverse phenotypic changes (Huang et al. 2003; Orphanides 2003). These reports provide qualitative evidence of the power of genomics to link phenotype with gene expression, thereby contributing to an understanding of mechanism of action. Some such reports demonstrate the predictive power of these data to classify compounds. However, they fail to address adequately quantitative dose- and time-dependent (e.g., threshold) responses that are the hallmark of toxicologic evaluation, making their immediate acceptance in regulatory arenas circumspect.

Nonetheless, toxicogenomics data may eventually be useful in hazard and risk assessment if data quality and validity can be adequately substantiated. Some regulators are finding that these data have the potential to add to the body of knowledge about compound mechanism of action. With appropriate dose- and time-dependent measurements, gene and protein changes can be used to mark the molecular events that occur as an organism moves through the continuum from exposure to response. The obvious benefit is the identification of early markers of response, including responses that mark the point of departure from adaptation to toxicity. In addition, it may be possible to detect unforeseen effects at very low doses or in unexpected tissues (Brown et al. 2002). This is important because changes in gene or protein expression alone are not sufficient to differentiate toxicity from biologic adaptation after exposure to an exogenous compound. The challenge for predictive toxicology is to link changes in gene and protein expression to sequential changes in phenotype, both adaptive and adverse, in a manner that is consistent with the underlying biologic mechanisms. For example, gene expression profiling has been used to classify hepatotoxins based on mechanism of action and to differentiate early, presumably adaptive, responses from later responses that are reflective of toxicity (Hamadeh et al. 2002a, 2002b; Waring et al. 2001, 2003). The gene expression changes correlated well with changes in histopathology and clinical chemistry, supporting the liver as target organ for the test compounds.

Although good technical progress has been made in recent years, additional proof-of-principle studies are needed for the regulatory community to become more accepting of the use of toxicogenomics data as part of the regulatory decision-making process. It would be important to demonstrate, for instance, that toxicogenomics not only can confirm what is already known about specific compounds and toxic end points (i.e., phenotypic anchoring) but also can accurately predict toxicity for unknown compounds. The task is to present regulatory scientists with new knowledge gained from toxicogenomics approaches in a familiar context. Ideally, at least in the short term, the focus will be the identification of single, or small sets of, genes or proteins that serve as biomarkers of response, as opposed to signatures of response that are the typical output of microarray experiments. Simple biomarkers of response are favored over complex expression signatures because they are familiar in toxicology assessment, are easy to maintain over time (e.g., are independent of the microarray platform), and can be readily validated. Validation strategies for toxicogenomics-based markers can be modeled after protocols for existing biomarkers. Thus, global gene expression technologies such as microarrays can be used to identify a specific gene marker,